

# THE KNOT MERIDIANS OF (1,1)-KNOT COMPLEMENTS ARE CTF-DETECTED

QINGFENG LYU

ABSTRACT. For any (1,1)-knot in a lens space, we construct a co-oriented taut foliation in its complement that intersects the boundary torus transversely in a suspension foliation of the knot meridian, or the infinity slope. This provides new evidence for a conjecture made by Boyer, Gordon and Hu using slope detections, related to the L-space conjecture.

## 1. INTRODUCTION

In [BGH21], the idea of slope detections is proposed to investigate the L-space conjecture for toroidal manifolds. In particular, they describe slopes realized by co-orientable taut foliations as “CTF-detected”:

**Definition 1.1** ([BGH21], Definition 5.1). Let  $M$  be a 3-manifold with  $\partial M \cong T^2$ . A *boundary slope*  $[\alpha]$  is an element in the projective space of  $H_1(\partial M, \mathbb{R})$ . It is *CTF-detected* if there exists a co-oriented taut foliation  $\mathcal{F}$  of  $M$  intersecting  $\partial M$  transversely s.t.  $\mathcal{F}|_{\partial M}$  is a suspension foliation of the slope  $[\alpha]$  (that is, a Reebless foliation with a closed leaf of slope  $[\alpha]$ ).

In [Eft18] it is proved that no toroidal integer homology sphere is an L-space. According to the L-space conjecture, we would expect that all toroidal integral homology spheres admit co-orientable taut foliations. By the gluing result in [BGH21] (Theorem 5.2), one can prove this by analysing the CTF-detected slopes of homology solid tori. More precisely they conjectured that

**Conjecture 1.2** ([BGH21], Conjecture 1.6). *Let  $M \not\cong S^1 \times D^2$  be an irreducible rational homology solid torus whose longitude  $\lambda_M$  is integrally null-homologous, then each rational slope of distance 1 from  $\lambda_M$  (any such slope is called **meridional**) is CTF-detected.*

[BGH21] proved this conjecture for  $M$  fibering over the circle. In particular this includes all fibered knot complements.

In the case  $M$  is the complement of a knot, there is a canonical choice of *meridional slope*, representing the meridian of the knot. In this paper we prove the following result:

**Theorem 1.3.** *If  $M$  is the complement of a nontrivial (1,1)-knot in  $S^3$  or some lens space, then the boundary slope of  $M$  represented by the knot meridian is CTF-detected.*

Our result is restricted to the canonical choice of meridional slope determined by  $(L, K)$ , where  $K \subset L$  is the knot and  $L$  is the total space  $S^3$  or some lens space. We expect possible generalisations to other meridional slopes. In fact, according to the

input from Floer homologies, most of the other meridional slopes yield non L-space surgeries [OS10], and according to the L-space conjecture, we should expect the existence of taut foliations of the knot complement intersecting the boundary torus in *product* foliations of these slopes. On the other hand, for our knot meridian or the infinity slope, suspension foliations are the best result possible.

The current method is not sensitive to the homology of the total space, hence we do not expect direct generalisations beyond (1,1)-knots. For example, the +5 Dehn surgery on the trefoil knot gives a lens space  $L'$ . Then the trefoil knot complement is also the complement of a knot  $K'$  living in  $L'$ . But according to the L-space conjecture, the meridional slope of  $K'$  should not be CTF-detected, since there is a toroidal L-space obtained by gluing the longitude of another trefoil complement along this slope [HRW23].

**Organisation of the paper.** In section 2, we review the related theories of (1,1)-knots and branched surfaces, prove some technical lemmas, and construct our branched surface for a (1,1)-knot complement. In section 3, we use an inductive argument to show that our branched surface fully carries a lamination. In section 4, we turn this lamination into a taut foliation of the (1,1)-knot complement.

**Acknowledgements** The author owes many thanks to his advisor Tao Li for countless helpful conversations and tremendous support throughout the writing of this paper.

## 2. PREPARATIONS

**2.1. (1,1)-diagrams.** We recall some basic properties of (1,1)-knots and (1,1)-diagrams. A (1,1)-knot is a knot that can be represented by some (1,1)-diagram, or *doubly pointed Heegaard diagram of genus one*, denoted as  $(\Sigma, \alpha, \beta, z, w)$ , where  $\Sigma$  represents the torus,  $\alpha, \beta$  the curves of the Heegaard diagram and  $z, w$  the two basepoints. The knot is recovered by taking properly embedded, boundary-parallel arcs in each solid torus connecting the two basepoints while avoiding the compression disks. For the purpose of this paper we fix an orientation of  $\Sigma$  and assume the two curves  $\alpha, \beta$  are oriented.

Given  $(\Sigma, \alpha, \beta, z, w)$  a doubly pointed Heegaard diagram of genus 1, one can isotope the two curves  $(\alpha, \beta)$  into minimal position, so that every bigon contains one basepoint. The resulting (1,1)-diagram is called **reduced**. A reduced (1,1)-diagram is called **nontrivial** if there exist bigons.

For a reduced (1,1)-diagram, we can use a standard square to represent the torus  $\Sigma$ , and place the  $\alpha$  curve in **standard position** - the horizontal boundaries of the square (see Figure 1). Now  $\beta$  is cut into arcs, and we call the arcs connecting the same side of  $\alpha$  **rainbow arcs** and the other arcs connecting different sides **vertical arcs**. Notice the rainbow arcs are exactly those forming bigons with  $\alpha$ .

We now claim every bigon contains exactly 1 basepoint. Suppose  $\alpha$  is in standard position and there's a rainbow arc bounding two basepoints with  $\alpha$ . It follows that any bigon on the other side of  $\alpha$  cannot bound any basepoint, thus there's no rainbow arcs on the other side. But this is impossible, since the number of rainbow arcs on both sides of  $\alpha$  should be equal to make the number of  $(\alpha, \beta)$ -intersection

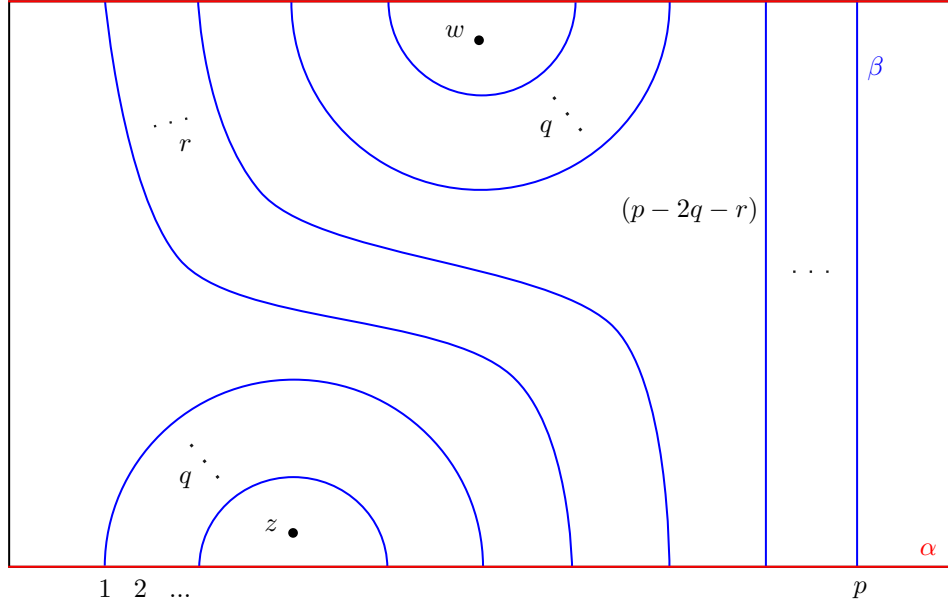


FIGURE 1. Reduced (1,1)-diagram parametrized by  $(p, q, r, s)$

points counted on both sides of  $\alpha$  equal. We also notice that each basepoint can only be bounded by rainbow arcs on the same side of  $\alpha$ .

It follows that the reduced (1,1)-diagram must look like Figure 1. According to the notation of [Ras05], the reduced diagram is then parametrized by a 4-tuple  $(p, q, r, s)$ , where  $p$  is the number of intersections of  $\alpha$  and  $\beta$ ,  $q$  is half the number of the rainbow arcs,  $r$  is the number of “leaning” vertical arcs (as depicted in the picture) and  $s$  is the twist occurred when identifying the horizontal boundaries  $\alpha$ , such that the first  $\beta$ -thread in the ceiling is connected to the  $(s + 1)$ -th  $\beta$ -thread on the floor.

We can regard the torus  $\Sigma$  with 2 basepoints  $(z, w)$  as a quotient orbifold of a genus-2 surface by a  $(\mathbb{Z}/2\mathbb{Z})$ -action generated by  $\tau$ , as shown in Figure 2.(a). Then the hyperelliptic involution of the genus-2 surface  $\tilde{h}$  descends to  $h$  a central reflection of the square representing  $\Sigma$ , exchanging the two basepoints, see Figure 2.(a)(b). On the other hand, we know the hyperelliptic involution  $\tilde{h}$  fixes all isotopy classes of simple closed curves, reversing orientations of the non-separating ones while preserving those of the separating ones [HS89]. Since  $\alpha$  and  $\beta$  are essential in  $\Sigma$ , their lifts are non-separating, and hence their orientations are reversed by  $h$ . Since the diagram obtained by doing central reflection is still reduced, we know  $(\Sigma, h(\alpha), h(\beta), z, w)$  is actually the same (1,1)-diagram with all orientations reversed. See Figure 2.(b). This gives us some important symmetry of the original diagram that we’ll use later.

We still need some additional analysis on the (1,1)-diagram for later use, which uses the fact that  $\alpha, \beta$  are essential simple closed curves. We consider the regions of  $\Sigma$  cut off by  $\alpha$  and  $\beta$ . Suppose  $\alpha$  is placed in standard position, then for any non-trivial (1,1)-diagram (as depicted in Figure 1), there are two bigons each containing one basepoint, two hexagon or one octagon (depending on whether there are two

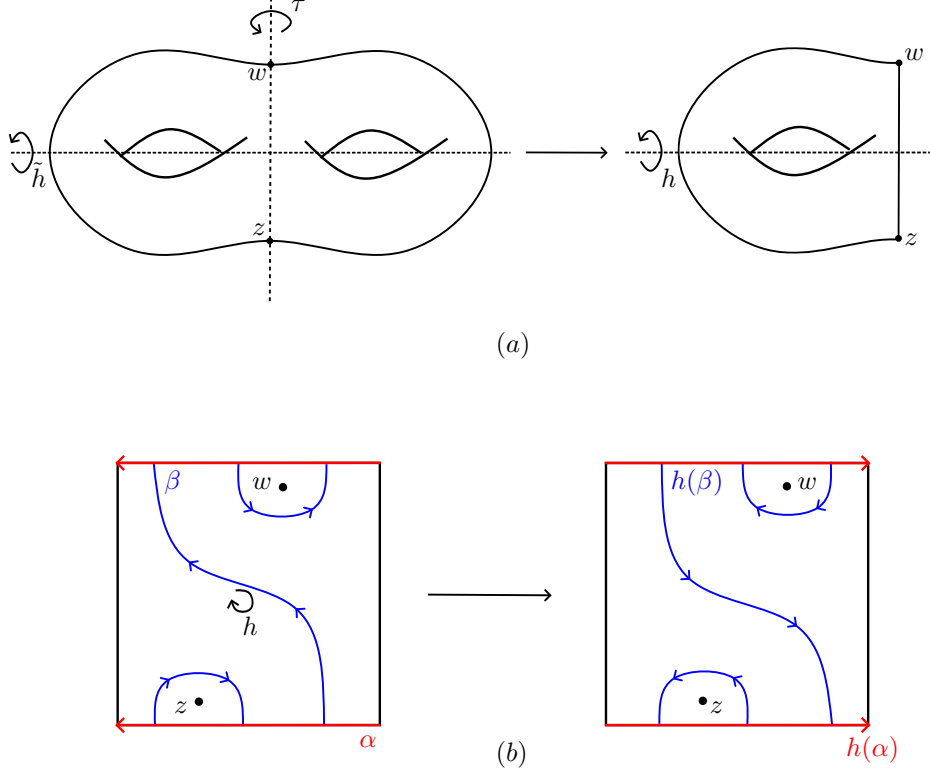


FIGURE 2. Hyperelliptic involution

kinds or one kind of vertical arcs) bounded by both rainbow arcs and vertical arcs, and many quadrilaterals bounded by either rainbow arcs or vertical arcs. We remark that although we use the standard position of  $\alpha$  to identify these regions, the partition into these regions (that there are two bigons and mostly quadrilaterals) does not rely on the position of  $\alpha$ . From now on when we say bigons in a reduced (1,1)-diagram, we refer to the regions cut out by the  $\alpha$  and  $\beta$  curves, i.e. only the *innermost* bigons.

**Definition 2.1.** Fixing orientations of  $(\Sigma, \alpha, \beta)$ , for each  $\alpha$ -arc cut out by  $\beta$ , we say it is  $(\beta)$ -**sink** if it always lies to the left of the  $\beta$  curve at its endpoints,  $(\beta)$ -**source** if it always lies to the right of the  $\beta$  curve at endpoints, and  $(\beta)$ -**parallel** otherwise. See Figure 3  $a \sim c$ . It follows immediately that for a quadrilateral region its two boundary  $\alpha$ -arcs must be of the same type. We call it a  $(\beta)$ -**sink sector** if its boundary  $\alpha$ -arcs are sink, a  $(\beta)$ -**source sector** if its boundary  $\alpha$ -arcs are source, and a  $(\beta)$ -**parallel sector** otherwise. See Figure 3  $d \sim f$ . Besides, we call a bigon region a  $(\beta)$ -**sink bigon** if its boundary  $\alpha$ -arc is sink, and a  $(\beta)$ -**source bigon** if its boundary  $\alpha$ -arc is source.

*Remark 2.2.*

- One can also define  $\alpha$ -sink, source, parallel  $\beta$ -arcs by interchanging  $\alpha, \beta$  in the above definition. This allows us to define  $\alpha$ -sink, source, parallel sectors

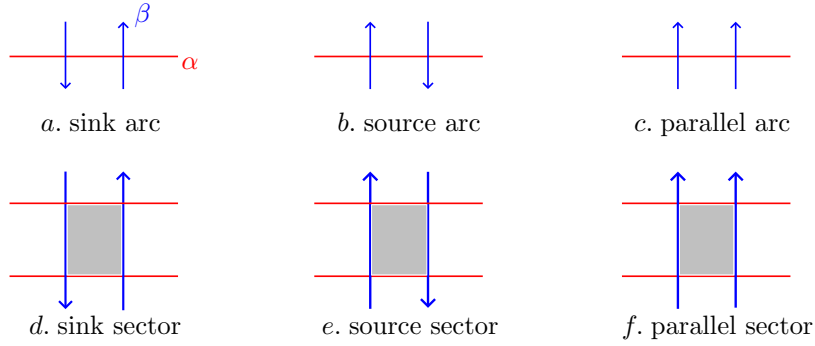


FIGURE 3. Arcs and sectors

and  $\alpha$ -sink, source bigons in the same sense. In later discussions we might omit the  $\alpha$ - or  $\beta$ - prefixes, as long as this does not cause confusion in the context.

- By the symmetry from hyperelliptic involution, if a bigon is  $\beta$ -sink, then the other bigon must be  $\beta$ -source and vice versa. In fact, the other bigon is obtained by taking hyperelliptic involution image of the original bigon and reversing the orientations of the boundary arcs. While the central reflection keeps the boundary  $\alpha$ -arc to be sink, reversing the orientation changes it from sink to source. It follows that there's exactly one  $\beta$ -sink bigon and one  $\beta$ -source bigon.

**Proposition 2.3.** *In a nontrivial (1,1)-diagram, there is a unique sink  $\alpha$ -arc and a unique source  $\alpha$ -arc among the boundary  $\alpha$ -arcs of the hexagons or octagon.*

*Proof.* First suppose we have two hexagons, and we look at their  $\alpha$ -boundary arcs. By enumeration we know there are either 0 parallel  $\alpha$ -arcs (when the oriented  $\beta$ -arcs form a “cycle”) or 2 parallel  $\alpha$ -arcs (when the  $\beta$ -arcs form a “cocycle”), see Figure 4. We claim that it must be the second case. In fact, if there is a hexagon with all 3 boundary  $\alpha$ -arcs sink (resp. source), then by the symmetry from hyperelliptic involution the other hexagon would have all 3 boundary  $\alpha$ -arcs source (resp. sink). Now since  $\beta$  is an essential simple closed curve in  $\Sigma$ , the two hexagons should be connected by pasting regions along the  $\alpha$ -arcs. In particular the regions connecting the hexagons should be some (possibly zero) quadrilaterals. However, along quadrilaterals sink  $\alpha$ -arcs can only connect to sink  $\alpha$ -arcs by pasting along the sink sectors, so the two hexagons cannot be connected by such pastings. This contradiction implies that each hexagon has 2 parallel boundary  $\alpha$ -arcs, plus 1 sink arc or 1 source arc. By hyperelliptic involution again, there is exactly 1 sink arc and 1 source arc.

In the case of having one octagon, we claim that the number of its sink  $\alpha$ -arcs must be odd. In fact, when counting sink  $\alpha$ -arcs by regions, each sink  $\alpha$ -arc is counted twice and we should eventually get an even number; on the other hand, the sink sectors contribute 2 each and the single sink bigon contributes 1 (see Remark 2.2), so the octagon should also contribute an odd number. Moreover, by the symmetry from hyperelliptic involution the number of sink and source boundary  $\alpha$ -arcs of the octagon must be equal, so there must be a unique sink and a unique source boundary  $\alpha$ -arc.  $\square$

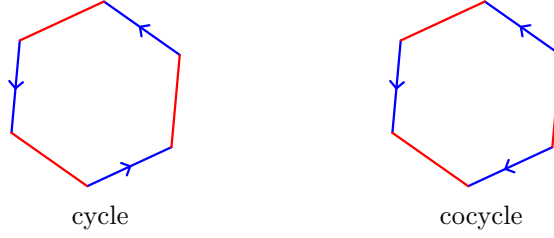
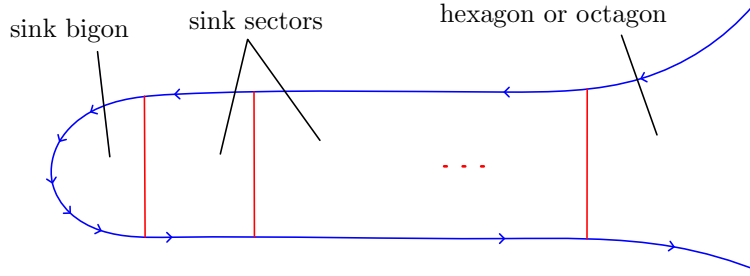


FIGURE 4. Hexagons

The boundary sink  $\alpha$ -arc of the sink bigon connects the bigon to a sink sector or the sink  $\alpha$ -arc of the hexagon or octagon. If connected to a sink sector, the other boundary  $\alpha$ -arc of the sink sector is then connected to another sink sector or the hexagon or octagon. It follows that the sink bigon is eventually connected to the sink  $\alpha$ -arc of the hexagon or octagon by pasting sink sectors along the boundary  $\alpha$ -arcs, see Figure 5. Similar things happen for the source case.

**Definition 2.4.** In a nontrivial (1,1)-diagram, the  $(\beta)$ -**sink tube** is the union of  $(\beta)$ -sink sectors that connect the  $(\beta)$ -sink bigon to the sink boundary  $\alpha$ -arc of the hexagon or octagon, see Figure 5. The  $(\beta)$ -**source tube** is the subregion of  $(\beta)$ -source sectors that connect the  $(\beta)$ -source bigon to the source boundary  $\alpha$ -arc of the hexagon or octagon.

FIGURE 5.  $(\beta)$ -sink tube

Notice that by Proposition 2.3 the sink and source tubes are well defined for the (1,1)-diagram. It also follows almost immediately from the definition that

**Proposition 2.5.** *The  $(\beta)$ -sink (resp. source) tube contains all  $(\beta)$ -sink (resp. source) sectors.*

*Proof.* For each  $(\beta)$ -sink sector, along the boundary  $\alpha$ -arcs it can only connect to another sink sector, the sink bigon, or the sink  $\alpha$ -arc of the hexagon or octagon. It follows that by pasting sectors along the  $\alpha$ -arcs it eventually must have one end connecting to the sink bigon and the other end connecting to the hexagon or octagon, thus lies in the sink tube. Similar argument works for the source case.  $\square$

**2.2. Branched surfaces.** Our main tool of constructing laminations and foliations would be the branched surfaces. Recall that a **branched surface**  $\mathcal{B}$  is a compact space locally modelled on Figure 6.(a). The subset of points that have no neighborhood isomorphic to  $\mathbb{R}^2$  is called the **branch locus**  $L(\mathcal{B})$ . According to the local

picture we can think of the branch locus as a collection of transversely-intersecting immersed curves in  $B$ . In this paper we sometimes refer to the immersed curves as **cusp curves**, as they look like cusps in certain complement of the branched surface. Points where the immersed curves intersect are called **double points**. Away from the double points, we can define the **branch direction** on branch locus up to homotopy, s.t. the direction is tangent to the branched surface, transverse to the branch locus, and always points to the side with fewer components, see Figure 6.(a). Connected components of  $\mathcal{B} - L(\mathcal{B})$  are called **sectors** of the branched surface. The branched surface is called **co-oriented** if each sector is orientable, and assigned with an orientation so that these orientations agree at the branch locus, see Figure 6.(a).

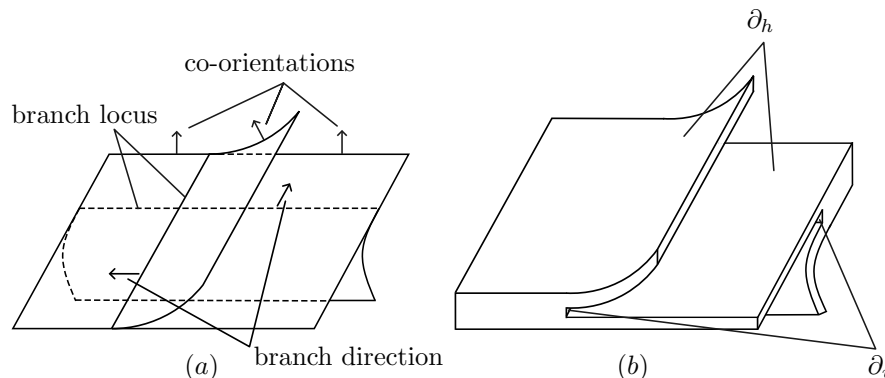


FIGURE 6. Branched surface and its regular neighborhood

For a branched surface  $\mathcal{B}$ , we can define its regular neighborhood  $N(\mathcal{B})$  to be an  $I$ -bundle over the branched surface. This can be constructed by taking trivial  $I$ -bundle for each sector and then paste them along the branch locus so that  $N(\mathcal{B})$  is locally modelled on Figure 6.(b). We can then define the **horizontal boundary**  $\partial_h N(\mathcal{B})$  to be the boundary of  $N(\mathcal{B})$  coming from the boundary of the fibers, and the **vertical boundary**  $\partial_v N(\mathcal{B})$  to be the remaining boundary of  $N(\mathcal{B})$  coming from the branch locus and possible boundary of the branched surface. For a branched surface with circle boundary, the horizontal boundary is some disjoint union of compact oriented surfaces and the vertical boundary disjoint union of annuli.

As we regard  $N(\mathcal{B})$  as an  $I$ -bundle over  $\mathcal{B}$ , there is a bundle projection  $\pi : N(\mathcal{B}) \rightarrow \mathcal{B}$  collapsing the fibers. Notice that  $\pi(\partial_v N(\mathcal{B})) = L(\mathcal{B}) \cup \partial\mathcal{B}$ .

An important bridge between branched surfaces and foliations would be the laminations. A lamination here is a closed subset of a 3-manifold foliated by (possibly noncompact) properly embedded surfaces. A lamination  $\mathcal{L} \subset N(\mathcal{B})$  is said to be *fully carried* by  $\mathcal{B}$  if it is transverse to the  $I$ -fibers and has projection image  $\pi(\mathcal{L}) = \mathcal{B}$ . After possibly replacing these surfaces by (surface  $\times I$ ) and taking (surface  $\times \partial I$ ), we can isotope the lamination so that  $\partial_h N(\mathcal{B}) \subset \mathcal{L}$  (or equivalently, retract the horizontal boundary onto  $\mathcal{L}$  along the fibers).

Once  $\partial_h N(\mathcal{B}) \subset \mathcal{L}$  for  $\mathcal{B}$  co-oriented, we know that the metric completion  $N(\mathcal{B})_{\mathcal{L}}$  of the complement  $N(\mathcal{B}) - \mathcal{L}$  is a disjoint union of trivial  $I$ -bundles over oriented surfaces, and thus  $\mathcal{L}$  can be trivially extended to a foliation  $\mathcal{F}$  of  $N(\mathcal{B})$ , transverse to the  $I$ -fibers.

It follows that to construct a foliation, sometimes it suffices to construct a branched surface that fully carries a lamination. However, usually such foliations may not be taut. Historically, [GO89] introduced essential laminations as an analog of taut foliations, and discussed when laminations fully carried by certain branched surfaces are essential.

**Definition 2.6.** A lamination  $\mathcal{L}$  in a 3-manifold  $M$  is called *essential* if

- (i) it contains no sphere leaf,
- (ii) leaves of  $\mathcal{L}$  are incompressible and end-incompressible, and
- (iii) components of  $M_{\mathcal{L}}$  (metric completion of  $M - \mathcal{L}$ ) are irreducible.

[GO89] found that, if a branched surface satisfies certain “incompressible conditions”, and has no disk of contact (a *disk of contact* is a disk  $D \subset N(\mathcal{B})$  transverse to the fibers and s.t.  $\partial D \subset N_v(\mathcal{B})$ ), then it only fully carries essential laminations. However, such branched surfaces may as well don’t fully carry any lamination. This was later improved in [Li02], by defining the *laminar branched surfaces*:

**Definition 2.7.** A branched surface  $\mathcal{B}$  in a closed, oriented 3-manifold  $M$  is called *laminar* if

- (i)  $\partial_h N(\mathcal{B})$  is incompressible in  $M - \text{int}(N(\mathcal{B}))$ , no component of  $\partial_h N(\mathcal{B})$  is a sphere, and  $M - \text{int}(N(\mathcal{B}))$  is irreducible (where  $\text{int}(X)$  is the interior of  $X$ ),
- (ii) there is no monogon in  $M - \text{int}(N(\mathcal{B}))$ ,
- (iii) there is no Reeb component (i.e.  $\mathcal{B}$  does not carry any torus that bounds a solid torus in  $M$ ), and
- (iv) there is no sink disk (a *sink disk* is a branch sector where branch directions at boundary always point inwards, see Figure 7).

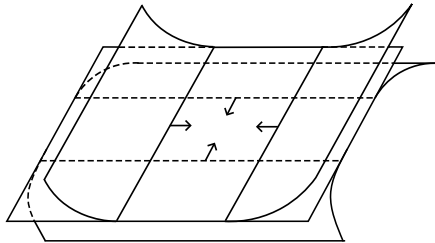


FIGURE 7. Sink disk

Conditions i) to iii) here are exactly the “incompressible conditions” suggested in [GO89], where i) corresponds to incompressibility and ii) corresponds to end-incompressibility. The improvement comes from iv), in that

**Theorem 2.8** ([Li02], Theorem 1). *Laminar branched surfaces in closed, oriented 3-manifolds fully carry laminations.*

Since laminar branched surfaces have no disk of contact ([Li02], Lemma 2.2), it follows immediately that the laminations carried are essential. On the other hand, if we do not require the laminations to be essential, we can drop certain “incompressible conditions” of the branched surface. In particular we will use the following lemma:

**Lemma 2.9.** *Let  $\mathcal{B}$  be a co-oriented branched surface with circle boundary. If  $\mathcal{B}$  is sink disk free, not carrying any torus, and no component of its horizontal boundary is a disk or a sphere, then  $\mathcal{B}$  fully carries a lamination.*

*Proof.* We can sew in a punctured genus 2 surface to each circular boundary to get a branched surface  $\mathcal{B}'$  without boundary. Consider the regular neighborhood  $N(\mathcal{B}')$ . Since still no component of horizontal boundary is a disk or a sphere, all components of  $\partial N(\mathcal{B}')$  must have Euler characteristic  $\leq 0$ . It follows that we can cap these boundary components off by pasting some irreducible 3-manifolds with incompressible boundary. Now  $\mathcal{B}'$  is laminar in the resulting closed 3-manifold (no monogons since co-oriented), thus fully carries a lamination by Theorem 2.8.  $\mathcal{B}$  as a subsurface also fully carries a lamination.  $\square$

We also quote a gluing lemma by Gabai here, which is actually used in [Li02] to prove the main theorem.

**Lemma 2.10** ([Gab92], Operation 2.4.4, modified in [Li02], Lemma 3.4). *Let  $\mathcal{B}$  be a branched surface with circle boundary. Suppose  $\mathcal{B}$  fully carries a lamination without disk leaves. Let  $c_1, c_2$  be two boundary components of  $\mathcal{B}$ . Then the branched surface  $\mathcal{B}'$  obtained by gluing  $c_1$  and  $c_2$  also fully carries a lamination.*

**2.3. Branched surfaces associated to nontrivial (1,1)-diagrams.** Now we define a branched surface associated to a nontrivial (1,1)-diagram, which we'll eventually prove to fully carry a lamination. The construction is inspired by [Li24].

**Definition 2.11.** Let  $(\Sigma, \alpha, \beta, z, w)$  be a nontrivial reduced (1,1)-diagram. We orient the two curves so that the boundaries of the two innermost bigons appear clockwise and anti-clockwise respectively (recall we fix an orientation of  $\Sigma$ ). We call the clockwise bigon *source bigon* and the anticlockwise one *sink bigon*. Notice our definition here complies with our earlier definitions of  $(\alpha, \beta)$ -sink and source, in the sense that the source bigon is both  $\alpha$ -source and  $\beta$ -source, and the sink bigon both  $\alpha$ -sink and  $\beta$ -sink.

We construct a branched surface from the torus  $\Sigma$  and the two compression disks bounded by  $\alpha, \beta$  on different sides of  $\Sigma$  (we call them  $\alpha$ - and  $\beta$ -**disks** respectively). Smooth the disks according to orientations so that branch direction points to the left-hand side (when observing on the oriented torus). Then remove the interior of the source bigon and a small disk in the interior of the sink bigon (one can think of this as puncturing a hole in the sink bigon). The resulting branched surface is called the *branched surface associated to the (1,1)-diagram*.

*Remark 2.12.* It is a general argument that after removing a source disk (i.e. a branch sector where branch directions at boundary always point outwards) we would get a new branched surface. Moreover, the branch locus of the new branched surface would be the original branch locus minus the boundary of the source disk. See Figure 8.

From now on unless otherwise specified, we'll assume our reduced (1,1)-diagrams are **oriented so that there exists an associated branched surface**. Notice that the two possible orientations here for a non-oriented reduced (1,1)-diagram (to have an associated branched surface) differ by the hyperelliptic involution, hence the associated branched surfaces are actually homeomorphic (with homeomorphism induced by the homeomorphism of the diagrams). Hence it makes sense for us to

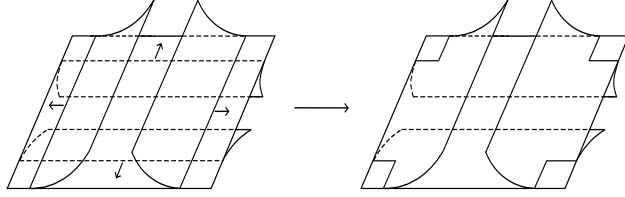


FIGURE 8. Removing a source disk

talk about the branched surface associated to a nontrivial reduced  $(1,1)$ -diagram, without specifying its orientations in advance.

Usually when constructing (taut) foliations using branched surfaces, one needs to extend the foliation from the branched surface neighborhood  $N(\mathcal{B})$  to the desired 3-manifold  $M$ . With our construction this is quite easy:

**Lemma 2.13.** *Let  $\mathcal{B}$  be the branched surface associated to a nontrivial reduced  $(1,1)$ -diagram  $(\Sigma, \alpha, \beta, z, w)$ . Then its regular neighborhood  $N(\mathcal{B})$  is homeomorphic to the corresponding  $(1,1)$ -knot complement.*

*Proof.* Let  $L$  be the total lens space or 3-sphere where the  $(1,1)$ -knot lives in. From the construction of  $\mathcal{B}$  there's a canonical way of embedding our branched surface into  $L$ , identifying  $\Sigma$  and the  $\alpha, \beta$ -disks with the Heegaard torus and compression disks. We notice from the construction that in each of the two solid tori cut out by the Heegaard torus  $\Sigma$ , the complement of the branched surface is a 3-ball obtained by cutting the solid torus along the compression disk. Moreover, there are two 1-handles connecting these two 3-balls at the removed source bigon and the hole in the sink bigon respectively. It follows that  $L - N(\mathcal{B})$  is a solid torus, with its core curve isotopic to the  $(1,1)$ -knot in  $L$ . Hence we can identify  $N(\mathcal{B})$  with the  $(1,1)$ -knot complement.  $\square$

We also prove the following lemma that'll be used in the next section:

**Lemma 2.14.** *The branched surface  $\mathcal{B}$  associated to a nontrivial  $(1,1)$ -diagram contains no disk of contact.*

*Proof.* First we show that there's only 1 cusp circle and 1 boundary circle in  $\mathcal{B}$  (that make up the vertical boundary of  $N(\mathcal{B})$ ). The boundary circle comes from the hole in the sink bigon. Before removing the source bigon, the branch locus of the model consists of two cusp circles  $\alpha$  and  $\beta$ . After removing the source bigon to get  $\mathcal{B}$ , the boundary of the source bigon is no longer part of branched locus. In fact, the branch locus becomes a single cusp circle obtained by connecting the remaining  $\alpha$ - and  $\beta$ -arcs at the vertices of the source bigon. Moreover, by isotoping along the compression disks we know on  $\partial N(\mathcal{B})$  the new cusp circle (as the core curve of the corresponding vertical boundary annulus) is still isotopic to the boundary of the source bigon. Hence both the cusp circle and the boundary circle represent the knot meridian. Since meridians of a nontrivial knot cannot bound disks in the knot complement (otherwise we'll be getting a non-separating 2-sphere in  $L$ ), there's no disk of contact in  $\mathcal{B}$ .  $\square$

### 3. CONSTRUCTING LAMINATIONS FROM $(1,1)$ -DIAGRAMS

In this section we use an inductive argument to prove the following statement:

**Proposition 3.1.** *Every branched surface associated to a nontrivial reduced (1,1)-diagram fully carries a lamination.*

**3.1. Primitive (1,1)-diagrams.** First we define primitive (1,1)-diagrams, and claim that the associated branched surfaces fully carry laminations. Recall that in Definition 2.1 we defined  $\beta$ -sink/source/parallel  $\alpha$ -arcs, and in Remark 2.2 following it  $\alpha$ -sink/source/parallel  $\beta$ -arcs.

**Definition 3.2.** Let  $(\Sigma, \alpha, \beta, z, w)$  be a reduced (1,1)-diagram. The diagram is called *primitive* if

- (i) any quadrilateral has  $(\beta)$ -parallel  $\alpha$ -arcs iff it has  $(\alpha)$ -parallel  $\beta$ -arcs, and
- (ii) if there are two hexagons, then for each hexagon the two non-parallel boundary arcs (one  $\alpha$ -arc and one  $\beta$ -arc) are next to each other.

When one of the curves is placed in standard position (recall our definition at the start of subsection 2.1, or see the  $\alpha$ -curve in Figure 1), there's a more direct description of being primitive. In fact, we have:

**Proposition 3.3.** *Let  $(\Sigma, \alpha, \beta, z, w)$  be a reduced (1,1)-diagram where  $\alpha$  is placed in standard position. Then the diagram is primitive iff*

- (i) *its rainbow arcs are in alternating direction, and*
- (ii) *its vertical arcs are in the same direction, see Figure 9.*

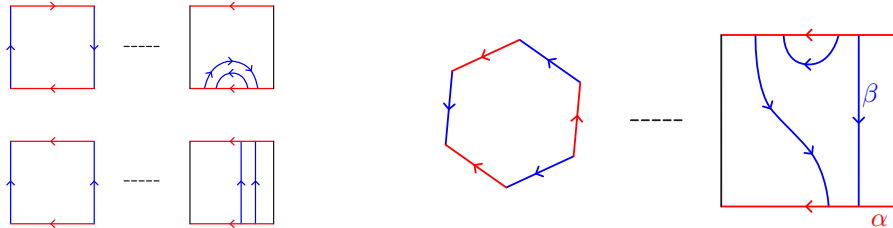


FIGURE 9. Quadrilaterals and Hexagons in primitive (1,1)-diagrams

*Proof.* Suppose the diagram is primitive and  $\alpha$  is in standard position. Quadrilaterals bounded by  $\alpha$  and the rainbow arcs then have non- $(\alpha)$ -parallel  $\beta$ -arcs, hence must have non- $(\beta)$ -parallel  $\alpha$ -arcs, as depicted in Figure 9 upper-left. It follows that the rainbow arcs must be alternating. On the other hand, quadrilaterals bound by  $\alpha$  and vertical arcs have parallel  $\beta$ -arcs, hence also have parallel  $\alpha$ -arcs, indicating that each kind of vertical arcs must be in the same direction (see Figure 9 bottom-left). It remains to show that if there are two kinds of vertical arcs, they also go in the same direction. Notice since there're two kinds of vertical arcs, there must be two hexagons. For each hexagon, the non- $(\alpha)$ -parallel  $\beta$ -arc must be the rainbow arc, see Figure 9 right. Now since the non- $(\beta)$ -parallel  $\alpha$ -arc is next to the rainbow  $\beta$ -arc, the opposite  $\alpha$ -arc bounded by vertical  $\beta$ -arcs must be parallel, indicating that the two kinds of vertical arcs are in the same direction.

One can check that these translations also work for the inverse direction of the statement. The proposition then follows.  $\square$

We remark that by our Definition 3.2 the diagram being primitive is independent of the position of the diagram, i.e. if we place  $\beta$  in standard position instead, we will still get alternating rainbow  $\alpha$ -arcs and vertical  $\alpha$ -arcs in the same direction.

**Proposition 3.4.** *Branched surfaces associated to primitive (1,1)-diagrams fully carry laminations.*

We defer the proof of this proposition to subsection 3.4, where we introduce what we call the “sink tube push” to eliminate the sink disks in the branched surface.

**3.2. Reducing (1,1)-diagrams to primitive.** Our induction relies on the following observation of (1,1)-diagrams:

**Definition 3.5.** Let  $(\Sigma, \alpha, \beta, z, w)$  be a reduced (1,1)-diagram. An essential curve  $\gamma$  is said to carry  $\alpha$  if

- (i) it is disjoint from and isotopic to  $\alpha$  in  $\Sigma$  (without the marked points  $z, w$ ),
- (ii) it only intersects the  $\alpha$ -parallel  $\beta$ -arcs.
- (iii)  $(\Sigma, \gamma, \beta, z, w)$  is also a reduced (1,1)-diagram.

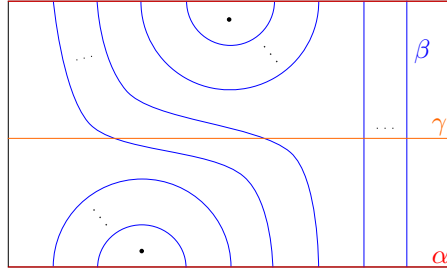


FIGURE 10. Carrying curve

*Remark 3.6.* When  $\alpha$  is placed in standard position, condition (ii) is equivalent to saying that  $\gamma$  only intersects vertical arcs, see Figure 10.

**Proposition 3.7.** *Let  $(\Sigma, \alpha, \beta, z, w)$  be a reduced (1,1)-diagram. Then there exists  $\gamma$  carrying  $\alpha$  and it is unique up to isotopy in the twice-punctured torus  $(\Sigma, z, w)$ .*

*Proof.* We can place  $\alpha$  in standard position. Then we claim the curve  $\gamma$  as depicted in Figure 10 is carrying  $\alpha$ . Conditions (i) and (ii) are easily checked. For (iii), notice that bigons bounded by  $\gamma$  and  $\beta$  must intersect  $\alpha$ , hence contain some bigon bounded by  $\alpha$  and  $\beta$ , hence must also contain some basepoint. It follows that the new (1,1)-diagram  $(\Sigma, \gamma, \beta, z, w)$  is also reduced.

For uniqueness, we first claim that each region cut off by  $\alpha$  and  $\beta$  has 0 or 2  $\alpha$ -parallel  $\beta$ -arcs. In fact, one can directly check that bigons have 0,  $\alpha$ -parallel quadrilaterals have 2, other quadrilaterals have 0, and the hexagons or octagons have 2 (recall Proposition 2.3). Now since  $\gamma$  is essential, it cannot be contained in a single region. Since it is disjoint from  $\alpha$ , it can only exit and enter regions at the  $\beta$ -arcs. Since it is closed, when it enters a region it must also exit it. Since the new (1,1)-diagram is reduced, it cannot exit at the same arc as entry (otherwise there will be a bigon with no basepoint). It follows that  $\gamma$  is characterized by a cycle of regions with  $(\alpha)$ -parallel  $\beta$ -arcs that it passes through, see Figure 11. Now place

$\alpha$  in standard position. As can be seen in Figure 10, there is a unique such cycle including all the regions with parallel  $\beta$ -arcs. This determines the unique (up to isotopy) curve  $\gamma$  carrying  $\alpha$ .  $\square$

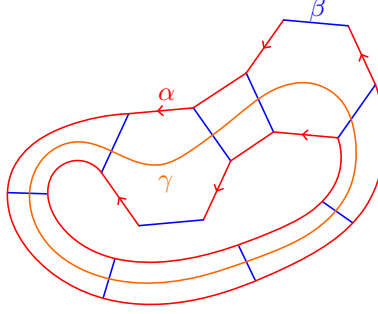


FIGURE 11. A cycle formed by regions with parallel  $\beta$ -arcs

*Remark 3.8.* Since the unique cycle formed by all regions with ( $\alpha$ -)parallel arcs characterizes the carrying curve (of  $\alpha$ ) up to isotopy, we can use this to find the carrying curve without having the original curve placed in standard position, see the  $\delta$ -curve carrying  $\beta$  in Figure 13.

Only nontrivial (1,1)-diagrams have associated branched surfaces. Hence our replacement with the carrying curves needs to guarantee that the new diagram is still nontrivial. This happens exactly when the (1,1)-diagram is not primitive.

**Proposition 3.9.** *If a reduced (1,1)-diagram  $(\Sigma, \alpha, \beta, z, w)$  is not primitive, with curves  $\gamma, \delta$  carrying  $\alpha, \beta$  respectively, then either  $(\Sigma, \gamma, \beta, z, w)$  or  $(\Sigma, \alpha, \delta, z, w)$  is nontrivial.*

*Proof.* Suppose  $\alpha$  is placed in standard position. Since the diagram is not primitive, there're either rainbow arcs bounding  $\beta$ -parallel sectors, or vertical arcs in different directions. In the first case, by Remark 3.8 the  $\delta$  curve passes through the  $\beta$ -parallel sector bounded by rainbow arcs (see Figure 13 for an example). It follows that the  $\delta$ -arc in this sector is a rainbow arc in  $(\Sigma, \alpha, \delta, z, w)$ , indicating non-triviality. In the second case, we first notice that as in Figure 10 the  $\gamma$  curve intersects all vertical arcs. Since the vertical arcs are not in the same direction, there exists some non- $\beta$ -parallel  $\gamma$ -arcs. Now if we place  $\beta$  in standard position instead, this  $\gamma$ -arc must be a rainbow arc (vertical arcs are parallel). It then follows that  $(\Sigma, \gamma, \beta, z, w)$  is nontrivial in this case.  $\square$

**3.3. Inductive construction of laminations.** In this subsection we'll try to prove the following proposition:

**Proposition 3.10.** *Let  $(\Sigma, \alpha, \beta, z, w)$  be a reduced (1,1)-diagram that is not primitive, with  $\delta$  carrying  $\beta$ . Suppose  $(\Sigma, \alpha, \delta, z, w)$  is nontrivial and its associated branched surface fully carries a lamination. Then the branched surface associated to  $(\Sigma, \alpha, \beta, z, w)$  also fully carries a lamination.*

The proof of this proposition relies on a series of constructions of branched surfaces. We'll introduce these constructions in several steps, and then show that in

each step the “fully carrying laminations” property is carried over. Lemmas 3.11 ~ 3.14 below will be proved later in this and the following subsections.

**Step 1: Attaching the  $\delta$ -annulus.** Let  $\mathcal{B}$  be the branched surface associated to  $(\Sigma, \alpha, \beta, z, w)$ . Consider the curve  $\delta$  on the torus. Pick an orientation of  $\delta$  so that the pair  $(\alpha, \delta)$  forms sink and source bigons. Now we can attach an annulus to  $\mathcal{B}$  by identifying one of its boundary components with the  $\delta$  curve, so that it is attached to  $\Sigma$  on the same side as the  $\beta$ -disk, and then smooth it according to the orientation, so that when observed on  $\Sigma$  the branch direction still points to the left of the  $\delta$ -curve direction. We call the resulting branched surface  $\mathcal{B}'$ .

**Lemma 3.11.** *If  $\mathcal{B}'$  fully carries a lamination, then so does  $\mathcal{B}$ .*

**Step 2: Taking the difference.** Let  $\mathcal{C}$  be the branched surface associated to  $(\Sigma, \alpha, \delta, z, w)$ . We can remove a small disk in the interior of the  $\delta$  disk to get a branched surface  $\mathcal{C}'$ . We can then think of the branched surface  $\mathcal{C}'$  as a sub-branched surface of  $\mathcal{B}'$  (i.e. there exists an embedding  $\mathcal{C}' \hookrightarrow \mathcal{B}'$  such that each sector of  $\mathcal{C}'$  is a union of sectors of  $\mathcal{B}'$ ). We consider the complement  $\mathcal{A} = \mathcal{B}' - \mathcal{C}'$ .  $\mathcal{A}$  consists of the  $\beta$ -disk and sectors on the torus corresponding to the  $(\alpha, \delta)$ -source bigon minus the  $(\alpha, \beta)$ -source bigon (see the shaded regions in Figure 13; notice the two bigons are always nested in this way, since when we place  $\alpha$  in standard position, the (innermost) rainbow  $\delta$ -arc exists (by nontriviality supposition of (1,1)-diagram) and is amid the rainbow  $\beta$ -arcs (lying in a  $\beta$ -parallel sector)).

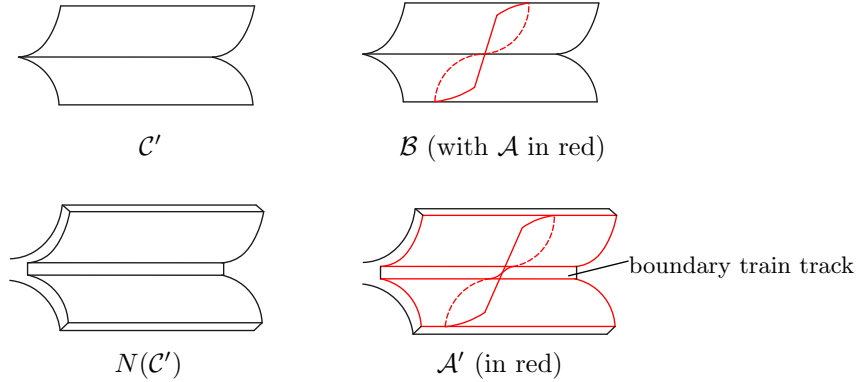


FIGURE 12. Attaching  $\mathcal{A}$  to  $\partial_h N(\mathcal{C}')$

$\mathcal{A}$  alone cannot pass on laminations, so we need some further constructions. We construct a branched surface  $\mathcal{A}'$  consisting of  $\mathcal{A}$  and the horizontal boundary  $\partial_h N(\mathcal{C}')$ , where  $\mathcal{A}$  intersects the two horizontal boundary components in the same branch direction as if intersecting with  $\mathcal{C}'$ , see Figure 12. Denote the two horizontal boundary components  $\partial_h^+$  and  $\partial_h^-$ . These are pairs of pants each with three boundary circles. We denote the boundary circles coming from the cusp of  $\mathcal{C}'$  as  $l_{\mathcal{C}'}^{\pm}$  (the  $\pm$  sign here indicates if it's the boundary circle of  $\partial_h^+$  or  $\partial_h^-$ ), the boundary circles in the sink bigon as  $l_s^{\pm}$ , and the boundary circles at the  $\delta$ -annulus as  $l_{\delta}^{\pm}$ . Suppose the  $\beta$ -disk (of  $\mathcal{A}$ ) is to be attached to  $\partial_h^+$ .

With  $\mathcal{A}'$  we then have the following lemma:

**Lemma 3.12.** *Suppose  $\mathcal{A}'$  and  $\mathcal{C}'$  fully carry laminations, then  $\mathcal{B}'$  also fully carries a lamination.*

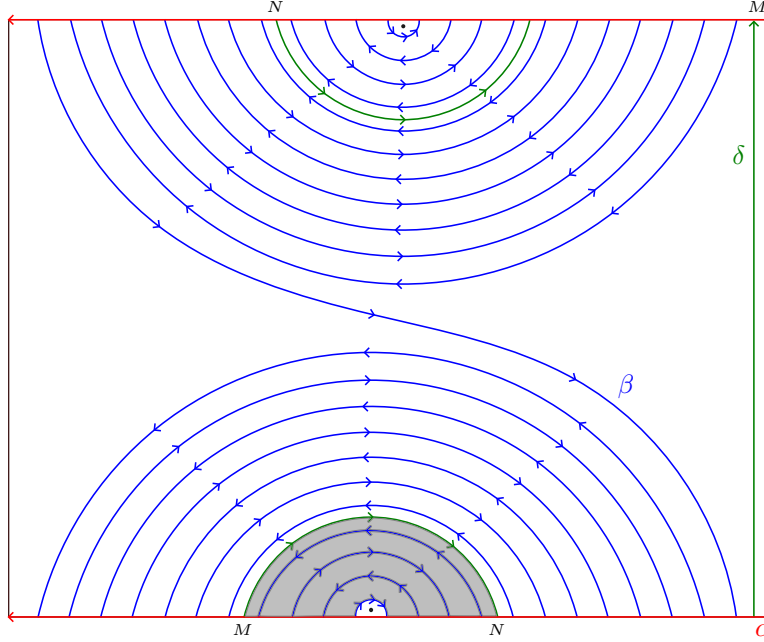


FIGURE 13. Knot (23,11,1,7)

**Step 3: Collapsing the boundary train track.** For technical reasons (to apply Lemma 2.9) we need to “collapse” the boundary train track of  $\mathcal{A}'$  to circles. Recall that  $\partial_h^\pm$  each has 3 boundary circles. When attaching  $\mathcal{A}$  to them to obtain  $\mathcal{A}'$ ,  $l_{\mathcal{C}'}^\pm$  are the only boundary circles that  $\mathcal{A}$  intersects. Hence besides the circle boundary components,  $\mathcal{A}'$  has a boundary train track at the  $\mathcal{C}'$ -cusp (one can spot this cusp on the (1,1)-diagram as  $\alpha \cup \delta - \partial((\alpha, \delta)$ -source bigon)), consisting of  $l_{\mathcal{C}'}^\pm$  and two short boundary arcs from  $\mathcal{A}$ , see Figure 12 and Figure 14 left. Denote the boundary train track as  $\mathcal{T}$ .

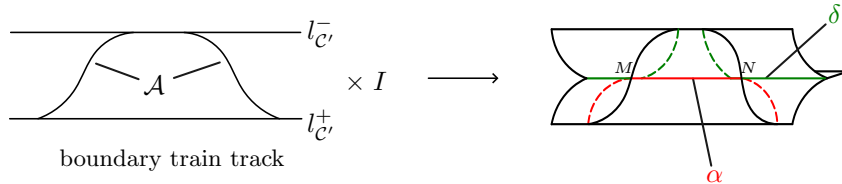


FIGURE 14. Collapsing at the  $\mathcal{C}'$ -cusp

Now we collapse/pinch  $\mathcal{T}$  into a single circle as shown in Figure 14. To give a detailed description, take a neighborhood of  $\mathcal{T}$  in  $\mathcal{A}'$  and denote it as  $\mathcal{T} \times I$  (as shown in Figure 14 left), with  $\mathcal{T} \times \{0\}$  representing the actual boundary of  $\mathcal{A}'$ . Our “collapse” is then described as a quotient operation on  $\mathcal{T} \times [0, 1/2]$ , where we keep the  $[0, 1/2]$  factor unchanged and quotient  $\mathcal{T}$ . More precisely, we map the two  $\mathcal{A}$ -arcs of the boundary train track to two points, and identify the corresponding  $l_{\mathcal{C}'}^\pm$ -arcs cut out by the  $\mathcal{A}$ -arcs. See Figure 14, where we note that after collapsing the two double points  $M, N$  (obtained by collapsing the  $\mathcal{A}$ -arcs) actually correspond to the vertices of the  $(\alpha, \delta)$ -source bigon (see them also in Figure 13).

The resulting branched surface  $\mathcal{A}'$  has a circle boundary at the  $\mathcal{C}'$ -cusp instead of a train track, and has branch locus 2 cusp circles (one is  $\delta$  and the other is  $(\alpha \cup \beta - \partial((\alpha, \beta)$ -source bigon)). See Figure 14 right, where the  $\alpha$ -locus is joined with  $\beta$  at the  $(\alpha, \beta)$ -source bigon away from the  $\mathcal{C}'$ -cusp).

**Lemma 3.13.**  $\mathcal{A}'$  fully carries a lamination if  $\mathcal{A}''$  does.

**Lemma 3.14.**  $\mathcal{A}''$  fully carries a lamination.

In this subsection we prove the first three Lemmas 3.11 ~ 3.13. We leave the proof of Lemma 3.14 to the next subsection 3.4 where we use splittings.

*Proof of Lemma 3.11.* By Proposition 2.13 we can identify  $N(\mathcal{B})$  with the knot complement. Recall from the proof of Lemma 2.14 that both the cusp circle and the boundary circle of  $\mathcal{B}$  represent the knot meridian on  $\partial N(\mathcal{B})$ . We claim that the  $\delta$  curve on  $\partial N(\mathcal{B})$  (where the  $\delta$ -annulus is to be attached) also represents the knot meridian. In fact, we can embed  $\mathcal{B}$  in the total space  $L$  canonically as described in the proof of Proposition 2.13, where the torus  $\Sigma$  serves as a Heegaard surface of  $L$ . Now since  $\delta$  is essential and disjoint from  $\beta$ , it is also a compression curve (of the Heegaard splitting of  $L$ ), and thus bounds a disk in  $L - N(\mathcal{B})$ . However, since  $\delta$  intersects  $\alpha$  in strictly less points than  $\beta$  (see Figure 10, where the carrying curve only intersects the vertical arcs),  $\delta$  and  $\beta$  are not isotopic on the twice-punctured torus  $(\Sigma, z, w)$ . It follows that on  $\Sigma$  the two annuli cut off by  $\beta$  and  $\delta$  would each contain a basepoint, see Figure 15. Hence the  $\delta$ -disk essentially intersects the knot once (in the solid torus  $L - N(\mathcal{B})$ ). Hence the  $\delta$  curve is essential on  $\partial N(\mathcal{B})$  and bounds a disk in  $L - N(\mathcal{B})$ , thus representing the knot meridian.

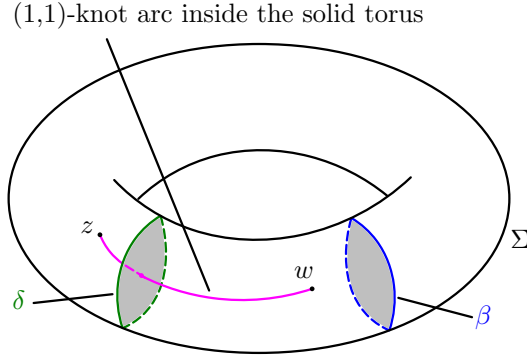


FIGURE 15. The  $\delta$ -disk and the (1,1)-knot

Denote the two horizontal boundary components of  $N(\mathcal{B})$  as  $\partial_h^{+'}, \partial_h^{-'}$ , so that the  $\delta$ -annulus is attached to  $\partial_h^{+'}$ . Since  $\delta$  also represents the knot meridian,  $\partial_h^{+'}$  is divided by  $\delta$  into two annuli. See the left two figures in Figure 16, where the top and bottom sink bigon holes are identified to form the boundary torus of  $N(\mathcal{B})$ . Now suppose  $\mathcal{B}'$  fully carries a lamination. According to the branch direction of  $\delta$  (see Figure 16), we can do different operations to eliminate the  $\delta$ -annulus and get a lamination fully carried by  $\mathcal{B}$ .

If the branch direction points to the cusp (Figure 16 top), we can attach a neighborhood of the boundary circle on the  $\delta$ -annulus to a neighborhood of the

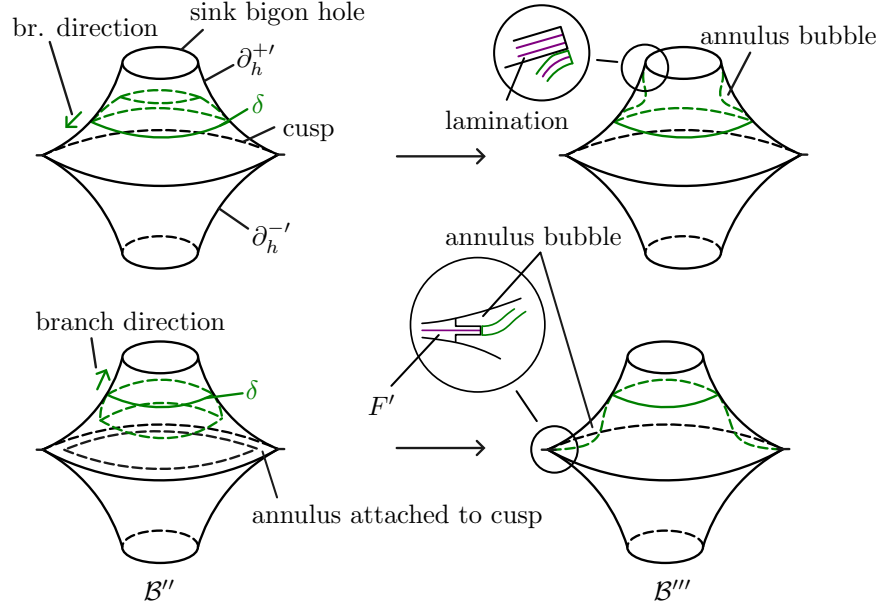


FIGURE 16. Eliminating annulus

boundary circle in the sink bigon. The new branched surface (as depicted in Figure 16 top-right) then fully carries a lamination while containing an annulus bubble. By collapsing the annulus bubble, the lamination collapses to become a lamination  $\mathcal{N}$  fully carried by  $\mathcal{B}$ .

Now suppose the branch direction points to the boundary circle in sink bigon (Figure 16 bottom). We show that we can still modify the lamination  $\mathcal{N}'$  fully carried by  $\mathcal{B}'$ . Recall after some isotopy we can assume that the metric completion of  $N(\mathcal{B}') - \mathcal{N}'$  consists of  $I$ -bundles. Consider the  $I$ -bundle whose boundary contains the vertical boundary corresponding to the cusp. Since our branched surface is transversely oriented, this  $I$ -bundle is some  $F \times [0, 1]$ , where  $F$  is oriented and has a circle boundary  $C$  corresponding to the cusp ( $F$  itself may have multiple boundary components). We can extend  $F \times \frac{1}{2}$  along  $C$  (i.e. attaching a small annulus to  $C$ ) and add this leaf  $F'$  to  $\mathcal{N}'$ . The resulting lamination  $\mathcal{N}'' = \mathcal{N}' \cup \{F'\}$  is fully carried by some branched surface  $\mathcal{B}''$  which is obtained by attaching an annulus to the cusp of  $\mathcal{B}'$  (see Figure 16 bottom-left). Since attaching (thickened) annuli along boundary does not change the topology of  $N(\mathcal{B})$ , we have  $N(\mathcal{B}'')$  also homeomorphic to the knot complement. Moreover, all its three boundary components (one each coming from the sink disk, the  $\delta$ -annulus, and the cusp) correspond to the knot meridian. Hence  $\mathcal{B}''$  cannot carry disks bounded by these boundary components. Now by the gluing lemma Lemma 2.10 we can glue the two boundary circles corresponding to  $\delta$  and cusp, and get a branched surface  $\mathcal{B}'''$  fully carrying a lamination (see Figure 16 bottom-right). One can then collapse the annulus bubble of  $\mathcal{B}'''$  to get  $\mathcal{B}$ , while the lamination is collapsed to some  $\mathcal{N}$  fully carried by  $\mathcal{B}$ .  $\square$

*Proof of Lemma 3.12.* We can glue  $\partial_h^\pm$  in  $\mathcal{A}'$  back to the corresponding horizontal boundary components of  $N(\mathcal{C}')$ . Now the lamination  $\mathcal{M}$  fully carried by  $\mathcal{A}'$  can

be regarded as a closed subset of  $N(\mathcal{B}')$ , containing surface leaves transverse to the  $I$ -fibers. However,  $\mathcal{M}$  is not yet a lamination of  $N(\mathcal{B}')$  since its leaves are not properly embedded at the  $\mathcal{C}'$ -cusp (recall that here  $\mathcal{A}'$  has a boundary train track  $\mathcal{T}$  as in Figure 14). The lamination  $\mathcal{M}$  intersects the vertical boundary annulus of  $N(\mathcal{C}')$  at the cusp in a 1-dimensional lamination.

Now by our supposition  $\mathcal{C}'$  fully carries a lamination  $\mathcal{L}$ . Similar as before, after some isotopy we can assume that the metric completion of  $N(\mathcal{C}') - \mathcal{L}$  consists of  $I$ -bundles, and that the  $I$ -bundle whose boundary contains the vertical annulus at  $\mathcal{C}'$ -cusp is some  $G \times I$  for  $G$  oriented surface. Moreover, since  $\mathcal{C}$  does not bound a disk of contact (Lemma 2.14), neither doesn't  $\mathcal{C}'$  (which is obtained by removing a disk from  $\mathcal{C}$ ). Hence  $G$  cannot be a disk. It is then a standard argument that  $G \times I$  can be given a lamination transverse to the  $I$ -fibers, s.t. when restricted to the boundary vertical annulus at the  $\mathcal{C}'$ -cusp it is any given 1-dimensional lamination. By setting the 1-dimensional lamination to be the same as that of  $\mathcal{M}$  at  $\mathcal{C}'$ -cusp, we can paste our lamination in  $G \times I$  to  $\mathcal{M}$  along the vertical annulus. We then get a lamination  $\mathcal{M}'$  carried by  $\mathcal{B}'$ . Now  $\mathcal{N}' = \mathcal{L} \cup \mathcal{M}'$  is a lamination fully carried by  $\mathcal{B}'$ .  $\square$

*Proof of Lemma 3.13.* We show that we can construct an embedding  $\mathcal{A}' \hookrightarrow \mathcal{A}''$ . Recall in the construction of  $\mathcal{A}''$  we only changed  $\mathcal{T} \times [0, 1/2] \subset \mathcal{A}'$  a small neighborhood of  $\mathcal{T}$ . The embedding can then be defined to be identity outside  $\mathcal{T} \times [0, 1]$ , while mapping  $\mathcal{T} \times [0, 1]$  to  $\mathcal{T} \times [3/4, 1]$  via linear map of the second factor. The lemma follows by restricting the lamination fully carried by  $\mathcal{A}''$  to  $\mathcal{A}'$ .  $\square$

**3.4. Splittings and rational tangles.** In this subsection we prove Proposition 3.4 and Lemma 3.14. In general we are to modify the branched surfaces to be sink disk free by splittings. We first recall some basic definitions.

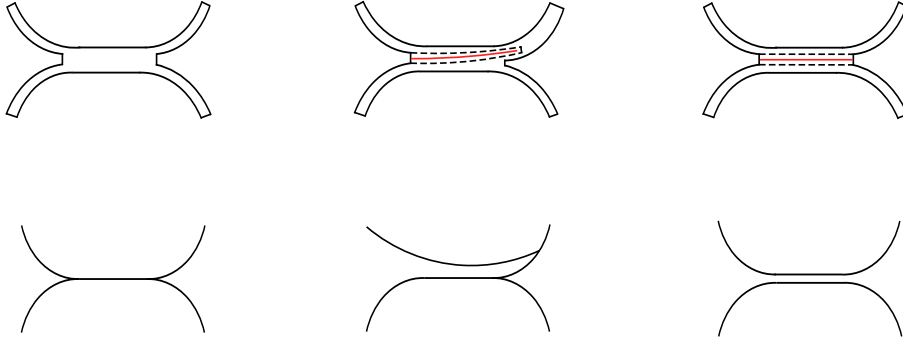


FIGURE 17. Splittings

A **splitting** of a branched surface  $\mathcal{B}$  along an oriented compact surface  $S \subset N(\mathcal{B})$  (where  $S$  is transverse to the  $I$ -fibers) results in a branched surface  $\mathcal{B}^S$ , such that there is an inclusion of  $I$ -bundle  $N(\mathcal{B}^S) \subset N(\mathcal{B})$  respecting the  $I$ -fibers, where  $N(\mathcal{B}) \setminus N(\mathcal{B}^S) = N(S) \cong S \times I$ . Notice that if  $\partial S \cap \partial_v N(\mathcal{B}) = \emptyset$ , then the splitting is just creating a bubble, so we generally hope this not to happen. Typically,  $S$  is a disk and  $\partial S$  intersects  $\partial_v N(\mathcal{B})$  in arcs, and the splitting is locally modelled on one of the pictures in Figure 17.

When the branched surface is obtained by pasting sectors (mostly disks in this paper) to a fixed surface  $\Sigma$ , we can describe the branch locus as curves on  $\Sigma$ . Then there is a special kind of splittings that gains importance in practice, which we call “**pushing arcs**”. These splittings are along disks and are locally modelled on the middle picture of Figure 17. When observed on  $\Sigma$ , it looks like that one arc (say, from curve  $\alpha$ ) is pushed over another arc (from  $\gamma$ ) onto the sector bounded by  $\gamma$ , and we say that the  $\alpha$ -arc is *pushed onto* the  $\gamma$ -arc. See Figure 18 for a 3-dimensional picture. We remark that one can also push arcs from the same curve.

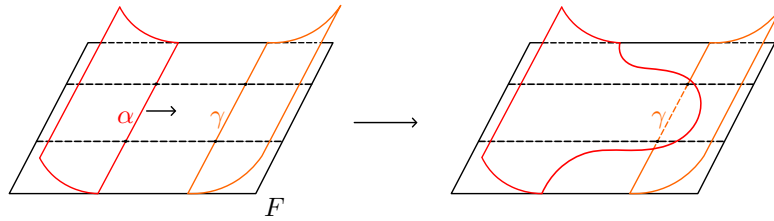


FIGURE 18. Pushing the  $\alpha$ -arc onto the  $\gamma$ -arc

The major advantage of talking about “pushing arcs” is that we can model these 3-dimensional operations on some 2-dimensional figure  $\Sigma$ , while the model fully reflects the operations on the branched surface. In this subsection unless specified we will talk about the operations on the 2-dimensional model rather than directly describing them on the branched surfaces.

Now we introduce what we call the “sink tube push”. Let  $(\Sigma, \alpha, \beta, z, w)$  be a nontrivial reduced (1,1)-diagram, and  $\mathcal{B}$  be its associated branched surface. Recall from Definition 2.4 and Proposition 2.5 the  $\beta$ -sink tube is the connected region containing all the  $\beta$ -sink sectors. This tube is bounded by two disjoint long  $\beta$ -arcs, which are connected by the sink bigon at one end of the tube. Now we consider the location of the source bigon (since it is removed, we generally cannot push the boundary arcs of it). The boundary  $\beta$ -arc of the *source* bigon belongs to at most one of the two long  $\beta$ -arcs of the sink tube. Suppose one long  $\beta$ -arc does contain the  $\beta$ -arc of the source bigon, then our “ **$\beta$ -sink tube push**” is to push the other  $\beta$ -arc *onto* this arc. See Figure 19 below for illustrations of this operation, where in (b) the dashed arcs are pushed *onto* the solid arcs (and are no longer on the surface  $\Sigma$ ).

*Remarks 3.15.*

- (1) Our  $\beta$ -sink tube push is only defined when one of the long  $\beta$ -arcs does contain the  $\beta$ -arc of the source bigon. For the proof in this subsection we always reduce to this situation when we need a sink tube push.
- (2) To define a  $\beta$ -sink tube push, we only need a branched surface where a (disk) sector is attached to a surface  $\Sigma$  along some (essential) curve  $\beta \subset \Sigma$ , and a well-defined “ $\beta$ -sink tube” from the information on  $\Sigma$ . Later this subsection we’ll define similar operations on branched surfaces modified from  $\mathcal{B}$ , and we may still call them “sink tube pushes”.

To check if a branched surface is sink disk free, we generally need to examine all its sectors. However, when there’s no “trivial” sink disk (we’ll explain this shortly),

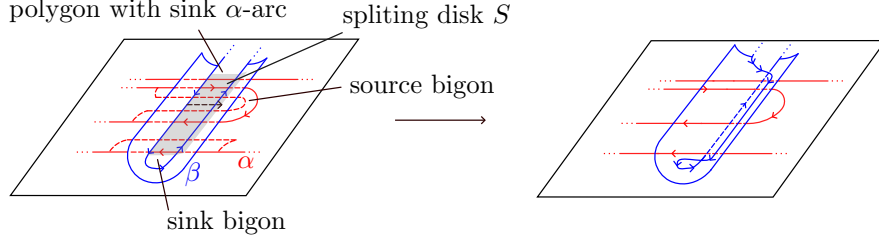
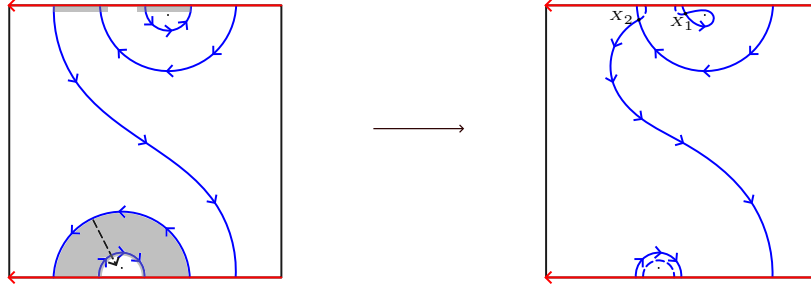
(a)  $\beta$ -sink tube push in branched surface(b)  $\beta$ -sink tube push in (1,1)-diagram (of  $4_1$ )

FIGURE 19. Sink tube push

we can instead examine the sink disk candidates around the double points. It turns out that there's only one candidate around each double point:

**Definition 3.16.** Let  $\mathcal{B}$  be a branched surface and  $X$  a double point in its branch locus. We say a branch sector  $D$  of  $\mathcal{B}$  is *around*  $X$  if  $X \in \partial D$ .

We can spot all sectors around  $X$  in a local picture of  $X$ , see Figure 6.(a). By enumerating these sectors, we can see that there is a unique sector  $D$ , s.t. there exists a neighborhood  $N(X)$  of  $X$ , where the branch locus arc  $N(X) \cap \partial D$  always has its branch direction pointing into  $D$ . See the upper-left corner of Figure 6.(a). We call this sector  $D$  the **sink corner** of the double point  $X$ .

**Lemma 3.17.** *Let  $\mathcal{B}$  be a branched surface. If the branch locus of  $\mathcal{B}$  does not contain a simple circle disjoint from others, then a sink disk of  $\mathcal{B}$  must be the sink corner of some double point.*

*Proof.* Suppose  $D$  is a sink disk of  $\mathcal{B}$ . If there's no double point in  $\partial D$ , then  $\partial D$  is a branch locus circle that's disjoint from other branch locus components, contradicting our supposition. Hence there's some double point  $X \in \partial D$ , and  $D$  is then the sink corner of  $X$ .  $\square$

Now we're in position to prove Proposition 3.4.

*Proof of Proposition 3.4.* Suppose  $(\Sigma, \alpha, \beta, z, w)$  is primitive and  $\alpha$  is placed in standard position. We first claim that, if we use the 4-tuple notation  $(p, q, r, s)$  as introduced in [Ras05] (see Figure 1) to identify the primitive (1,1)-diagram, then  $s$  is uniquely determined by  $(p, q, r)$ . We can look along  $\alpha$  at the signs of consecutive intersections (of  $\alpha$  and  $\beta$ ). At the rainbow arcs the signs are alternating; while at the vertical arcs the signs are the same. It follows that there's only one maximal

group of consecutive intersections of the same sign that contains more than one element (that is, the one containing all vertical arc intersections, see Figure 20 for an example, where the maximal group size is 2). Since we can observe this maximal group on both the roof and the bottom of the square, there's a unique legible way of gluing back the roof and the bottom, so that the maximal groups on the roof and the bottom are identified. This indicates that the gluing twist  $s$  is determined by  $(p, q, r)$  the parameters of the square. Moreover, in a primitive (1,1)-diagram the sink bigon and the source bigon would share an endpoint, since they're at the middle of the (maximal) alternating intersections, see Figure 20 and Figure 21.

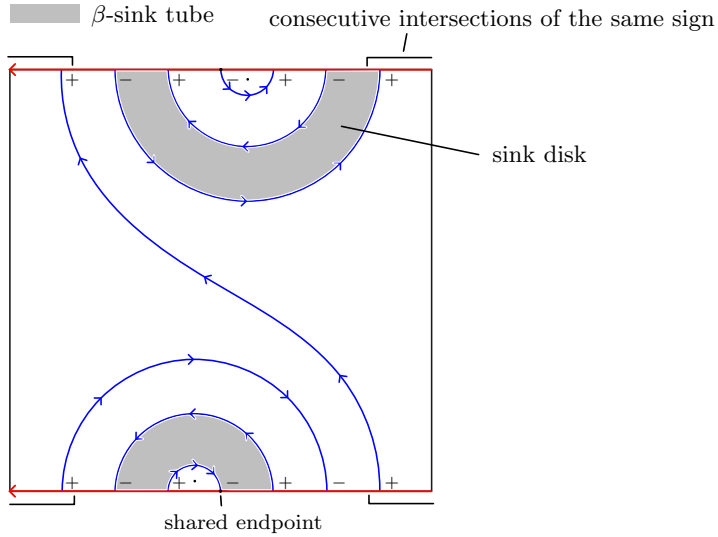


FIGURE 20. A primitive (1,1)-diagram for knot  $5_2$

There might be sink disks in the branched surface  $\mathcal{B}$  associated to  $(\Sigma, \alpha, \beta, z, w)$ . Recall that by our construction branch direction is always pointing to the left of the oriented curve, so a disk sector on  $\Sigma$  is a sink disk if and only if its boundary goes in the anti-clockwise direction, see Figure 20 for an example. In other words, it is a sink disk if and only if all its boundary arcs are ( $\alpha$ - or  $\beta$ -)sink. Since there's a hole in the sink bigon, all sink disks on  $\Sigma$  are sectors of the ( $\beta$ -)sink tube.

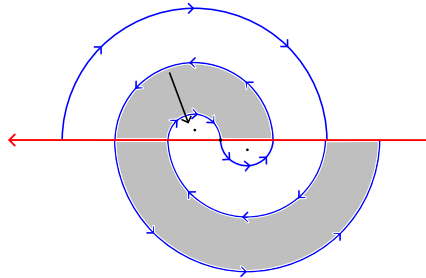


FIGURE 21. Sink tube spiral

If there are sink disks, we can then do a “sink tube push” to eliminate them. Since the sink and source bigons share an endpoint, by a short induction on the number of rainbow arcs we know the core of the sink tube must be a spiral along the rainbow arcs, see Figure 21. One then observes that all sink sectors bounded by rainbow arcs would have their “outer”  $\beta$ -arcs pushed. Hence after the operation all remaining rainbow arcs on  $\Sigma$  are of the same direction.

Now we can spot the double points of the branched surface  $\tilde{\mathcal{B}}$  after our operation and check their sink corners. The remaining intersections of  $\alpha$  and  $\beta$  on  $\Sigma$  still serve as double points; besides, the sink tube push would create two new double points,  $X_1$  in the sink bigon and  $X_2$  in the polygons. The sink corner of  $X_1$  is an annulus because of the hole in the sink bigon, thus not a sink disk. The sink corner  $D_2$  of  $X_2$  is a disk and actually comes from a polygon on the (1,1)-diagram. Now since our sink tube push does not move an entire vertical arc (we only moved entire arcs in the spiral),  $D_2$  still has a boundary  $\beta$ -arc that comes from a vertical arc on the (1,1)-diagram. Moreover, there are multiple such boundary  $\beta$ -arcs since one needs to go back to the same side of  $\alpha$  (i.e. roof or bottom) while traveling along  $\partial D_2$ . See Figure 19.(b) for an example, where  $D_2$  is actually bounded by the same “vertical” arc twice. Since our (1,1)-diagram is primitive, the vertical arcs are in the same direction, thus  $D_2$  also cannot be a sink disk. The sink corners of remaining  $(\alpha, \beta)$  intersections on  $\Sigma$  are all on the torus. If the sink corner has boundary  $\beta$ -arcs coming from vertical arcs, then as before there are multiple such boundary arcs and they are in the same direction; hence such a sink corner cannot be a sink disk. If the sink corner does not have boundary  $\beta$ -arcs coming from vertical arcs, then since it’s not a bigon, there are multiple “rainbow” boundary  $\beta$ -arcs, and they’re also in the same direction; such a sink corner also cannot be a sink disk.

The branch locus of  $\mathcal{B}$  is a single immersed curve obtained by joining  $\alpha$  and  $\beta$  at endpoints of the source bigon. It then follows that the branch locus of  $\tilde{\mathcal{B}}$  is still a single immersed curve. Now that we have examined the sink corners of all double points of  $\tilde{\mathcal{B}}$ , we can use Lemma 3.17 to conclude that  $\mathcal{B}'$  is sink disk free.

Since our splitting is locally modelled on Figure 17 middle, it does not change the topology of horizontal boundary, so  $\tilde{\mathcal{B}}$  still has horizontal boundary components 2 annuli. Since  $\mathcal{B}$  is transversely oriented with  $N(\mathcal{B})$  homeomorphic to the (1,1)-knot complement, any closed surface carried by  $\mathcal{B}$  is orientable and non-separating in the total space  $L$  (a transverse closed curve would connect the two sides). Since  $H_1(L, \mathbb{Q}) = 0$ , there is no such closed surface. In particular  $\mathcal{B}$ , thus  $\tilde{\mathcal{B}}$ , cannot carry any sphere or torus. Now by Lemma 2.9 our  $\tilde{\mathcal{B}}$  fully carries a lamination, thus  $\mathcal{B}$  also fully carries a lamination.  $\square$

It remains for us to prove Lemma 3.14. Our strategy is still to push arcs to eliminate sink disks, and then apply Lemma 2.9. In fact, the reason we modify the branched surface to  $\mathcal{A}''$  is that the sink disks (double points) are better controlled.

*Proof of Lemma 3.14.* We first find the sink disks in  $\mathcal{A}''$ . Recall from the construction that  $\mathcal{A}''$  has branch locus 2 cusp circles, one corresponding to  $\delta$  and the other  $(\alpha \cup \beta - (\alpha, \beta)$ -source bigon). Since the two circles does intersect at  $M, N$  vertices of the  $(\alpha, \delta)$ -source bigon (see Figure 14), by Lemma 3.17 we can just check the sink corners of the double points of  $\mathcal{A}''$ . The two double points  $M, N$  at the  $\mathcal{C}'$ -cusp share the same sink corner, which is the collapsed annulus at the cusp, not a sink

disk. The rest of the  $\delta$ -locus away from the  $\mathcal{C}'$ -cusp is the boundary of the  $(\alpha, \delta)$ -source bigon, where  $\mathcal{A}$  is attached to  $\partial_h^-$ . Notice this is the only part that  $\mathcal{A}$  is attached to  $\partial_h^-$ , so there's no other double point on  $\delta$ . Remaining branch locus not discussed contains roughly the boundary  $\alpha$ -arc of the  $(\alpha, \delta)$ -source bigon and the  $\beta$ -curve, minus the boundary of the  $((\alpha, \beta)$ -source bigon), at the vertices of which the two curves are joined (see Figure 22). If we place  $\alpha$  in standard position, then we can spot the double points, as the  $\beta$  curve intersects the  $(\alpha, \delta)$ -source bigon in alternating rainbow arcs, see the shaded region in Figure 13 or  $Q, R$  in Figure 22. One can see that the sink corners of double points like  $Q, R$  are candidates of sink disks of  $\mathcal{A}''$ , as in Figure 22.

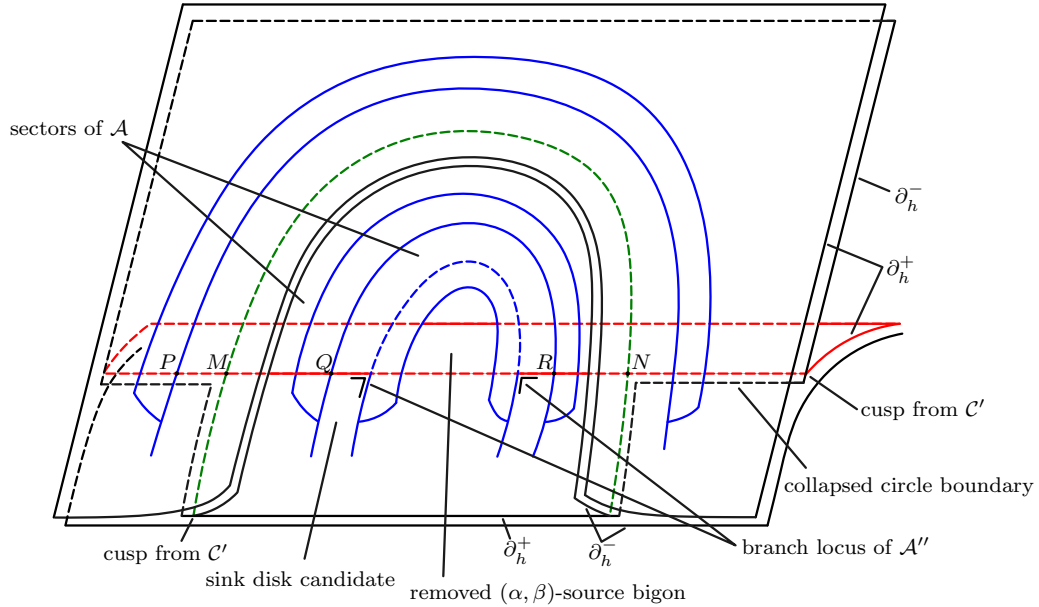


FIGURE 22.  $\mathcal{A}''$  near the  $(\alpha, \delta)$ -source bigon

**Remark**

- (1) The  $\beta$ -rainbow arcs inside the  $(\alpha, \delta)$ -source bigon must be alternating, since  $\delta$  passes through all parallel sectors.
- (2) In Figure 22,  $Q, R$  are double points of  $\mathcal{A}''$ . However,  $P$  is not a double point of  $\mathcal{A}''$ . In fact, here the red  $\alpha$ -locus is at the collapsed  $\mathcal{C}'$ -cusp, while the blue  $\beta$ -disk is attached to  $\partial_h^+$  away from the cusp, so the two loci don't actually intersect. **This is the very point for us to do all these inductive constructions.** By taking horizontal boundary  $\partial_h^\pm$  and attaching  $\mathcal{A}$  to them, we manage to separate the branch locus outside the  $(\alpha, \delta)$ -source bigon. As a result, we only need to take care of the double points inside the  $(\alpha, \delta)$ -source bigon, which is a lot easier.

Now we begin to push arcs to eliminate possible sink disks. Again, we'll be checking the double points. We call a double point **safe** if its sink corner is not a

sink disk. We'll do multiple splittings (pushing arcs) to show that in the end we can make all double points safe. We break up our splitting procedure into several steps:

**Step 1: Sink tube push on  $\mathcal{A}''$ .**

Recall that to define pushing arcs, we need to regard some sectors as attached to a fixed surface, and identify its boundary branch locus as some curves on the fixed surface. Now consider how the  $\beta$ -disk sector is attached to the rest of  $\mathcal{A}''$ . Roughly speaking we can still regard it as attached to a torus  $\Sigma^+$  along the  $\beta$ -curve, where outside the  $(\alpha, \delta)$ -source bigon  $\Sigma^+$  consists of sectors coming from  $\partial_h^+$ , and at the  $(\alpha, \delta)$ -source bigon  $\Sigma^+$  comes from sectors of  $\mathcal{A}$  (see Figure 22).

However, as one can observe in Figure 22, the torus  $\Sigma^+$  is actually cut along  $\delta$ . That being said,  $\Sigma^+$  actually has 2 boundary circles corresponding to  $\delta$ . One of them comes from the cusp of  $\mathcal{A}''$ , which we'll denote as  $\delta_{cusp}$  (see the green curve in Figure 22); the other is the  $\delta$ -boundary circle of  $\partial_h^+$  formerly denoted as  $l_\delta^+$ , which we now denote as  $\delta_{\partial_h}$ . Also, since we have removed the  $(\alpha, \beta)$ -source bigon, the boundary arc of it is no longer part of the branch locus. So to push  $\beta$ -arcs on  $\Sigma^+$ , we need to meet the following conditions:

- (1) we do not move the boundary arc of the  $(\alpha, \beta)$ -source bigon, and
- (2) we do not push the arc across  $\delta$ .

**Remark** We use  $\Sigma^+$  to denote the ‘‘torus’’, because on the one hand the torus is much like our torus  $\Sigma$  in the (1,1)-diagram, while on the other hand we will be only pushing the  $\beta$ -arc, so only considering one side of  $\Sigma$ .

If there's only 1  $\beta$ -arc in the  $(\alpha, \delta)$ -source bigon, then there's no double point besides  $M, N$  (vertices of the  $(\alpha, \beta)$ -source bigon are not double points), and the branched surface  $\mathcal{A}''$  is trivially sink disk free. Suppose there are multiple alternating  $\beta$ -arcs. Since the  $\beta$ -arcs are alternating, the  $(\alpha, \beta)$ -source bigon is adjacent to a  $\beta$ -sink sector (see Figure 22). Now we can do a ‘‘sink tube push’’ for  $\beta$ , according to the information of the  $(\alpha, \beta)$ -(1,1)-diagram (notice that the operation does not cross  $\delta$ , which only passes the polygons and  $\beta$ -parallel sectors of the  $(\alpha, \beta)$ -diagram).

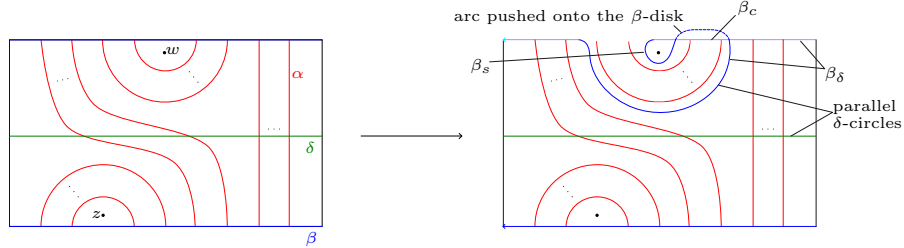


FIGURE 23.  $(\beta)$ -sink tube push for  $\beta$  in standard position

Remaining  $\beta$ -curve on  $\Sigma^+$  (that are not pushed onto the  $\beta$ -disk) consists of two loops (each with a double point cusp) and an arc connecting them, see Figure 23 where we place  $\beta$  in standard position instead. We denote the loop in the sink bigon  $\beta_s$ , the other loop  $\beta_\delta$ , and the connecting arc  $\beta_c$ . Notice that as shown in Figure 23,  $\beta_\delta$  is isotopic to  $\delta$  in the 2-pointed torus  $(\Sigma, z, w)$ , as they both intersect

each vertical  $\alpha$ -arc exactly once. Hence on  $\Sigma^+$  our  $\beta_\delta$  is actually isotopic to one of the  $\delta$ -boundary components of  $\Sigma^+$ .

The sink tube push produces two new double points  $X_s$  on  $\beta_s$  and  $X_\delta$  on  $\beta_\delta$ . The sink corner of  $X_s$  is an annulus because of the hole in the sink bigon. The sink corner of  $X_\delta$  is again an annulus, as in its branch direction  $\beta_\delta$  can be isotoped to one of the  $\delta$ -boundary circles of  $\Sigma^+$ , either  $\delta_{cusp}$  or  $\delta_{\partial_h}$ . Hence the two new double points are safe, and possible sink disks come from (sink corners of) double points at the intersection of  $\beta_c$  and the boundary  $\alpha$ -arc of the  $(\alpha, \delta)$ -source disk (i.e. the double points of  $\mathcal{A}''$  that remains on  $\Sigma^+$  after the sink tube push).

**Remark** Whether the boundary component (other than  $\beta_\delta$ ) of the sink corner of  $X_\delta$  is  $\delta_{cusp}$  or  $\delta_{\partial_h}$  depends on the number of alternating  $\beta$ -arcs inside the  $(\alpha, \delta)$ -source bigon. For example, in Figure 22, there is an even number of alternating  $\beta$ -arcs, so the branch direction of the outer  $\beta$ -arc containing  $P$  is pointing towards  $\delta$ , which then later becomes  $\beta_\delta$ , and the boundary component of sink corner is  $\delta_{\partial_h}$ .

### Step 2: Reduce $\beta_c$ to a rational tangle on a 4-basepoint sphere

We regret to say that Step 1 is not enough: there might still be sink disks left. To get a better characterization of how  $\beta_c$  intersects the  $\alpha$ -arc, and also to better describe our further splittings, we need to modify our model. We remark that the following ‘‘collapsing’’ operations are purely for simplifying our characterization, and don’t actually happen on our branched surface.

Recall that our  $\Sigma^+$  is actually cut along  $\delta$ , with two boundary  $\delta$ -circles  $\delta_{cusp}$  and  $\delta_{\partial_h}$ . Moreover, there is also a boundary circle in the sink bigon bounding the hole. Since we can never push arcs across these boundary circles, we can collapse(quotient) them to points. If we further mark the midpoint of the  $\alpha$ -arc in the  $(\alpha, \beta)$ -source bigon (which also cannot be moved by our pushing arcs operations), we get a sphere with 4 basepoints marked. We denote it by  $(S, a, b, c, d)$ , where  $S$  is the sphere we get,  $a$  is the midpoint of the  $\alpha$ -arc in source bigon,  $b$  is the  $\delta_{cusp}$  boundary circle,  $c$  is the  $\delta_{\partial_h}$  circle, and  $d$  is the boundary circle in the sink bigon, see the first four pictures of Figure 24, where we use knot  $(23,11,1,7)$  as an example and  $\alpha$  is placed in standard position.

Now as in the fourth picture of Figure 24, the  $(\alpha, \delta)$ -source bigon (see the shaded regions) becomes a bigon connecting two basepoints on  $S$ , bounded only by  $\alpha$ -arcs (that come from the boundary  $\alpha$ -arc of the source bigon). We can then collapse it to a *single* arc connecting the basepoints  $a, b$ . More precisely, the bigon can be parametrized by the unit disk, so that  $(\pm 1, 0)$  correspond to the vertices  $a, b$  and the  $\beta$  arcs intersecting the bigon are vertical; by collapsing we mean a projection of the unit disk to the  $x$ -axis. See this procedure in Figure 24 from the fourth picture to the fifth picture.

Recall again that after the sink tube push the  $\beta$ -arcs left on ‘‘ $\Sigma$ ’’ are two loops  $\beta_s, \beta_\delta$  and a connecting arc  $\beta_c$ . Now in our 4-point sphere  $(S, a, b, c, d)$ , each of the two  $\beta$ -loops bounds a small disk with a basepoint inside, and its branch direction points into the disk. We then further collapse(quotient) the loops and the disks they bound to the basepoints inside. Then  $\beta_c$  becomes an arc connecting the basepoint  $d$  to either  $b$  or  $c$ , and thus corresponds to a rational tangle. See the last two pictures in Figure 24.

We fix a frame so that  $\alpha$  represents the rational tangle  $\frac{1}{0}$ . Since  $\alpha, \beta$  come from a reduced  $(1,1)$ -diagram, their position on  $S$  is tight, i.e. having no trivial bigons.

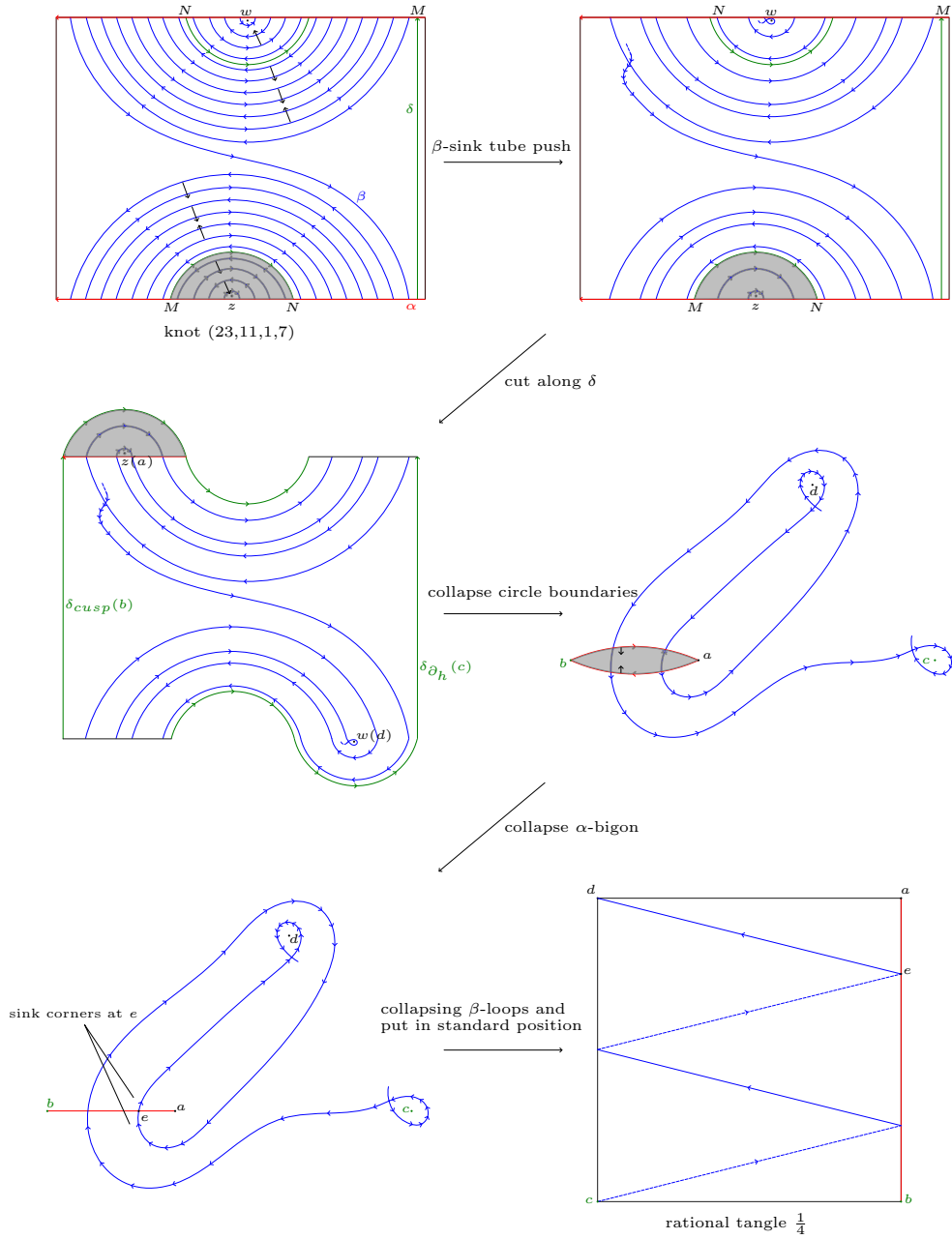


FIGURE 24. Rational tangle from knot (23,11,1,7)

Then  $\beta_c$  is actually characterized by a rational number  $r = \frac{p}{q}$ , where  $p, q \geq 0$ ,  $(p, q) = 1$ . In fact, we can place  $\beta_c$  in certain “standard position” as in Figure 24 bottom-right or Figure 25.(a), where the rectangle is bubbled to represent to sphere  $S$ . The boundary segments of the bubbled rectangle are chosen to be  $\frac{1}{0}$  and  $\frac{0}{1}$ . The solid  $\beta$ -segments are in the front of the bubbled rectangle, while the dashed

segments are on the back of it. If we regard the rectangle as the unit rectangle, then these segments are all of slope  $\pm \frac{p}{q}$ . We also recall that numbers  $p, q$  actually counts the total intersections of  $\beta_c$  with the  $\frac{1}{0}$  and  $\frac{0}{1}$  arcs respectively, where we count 2 for each intersection other than the basepoints, and 1 for each intersection at the basepoints.

We claim that our collapsings don't collapse possible sink disks. In fact, when quotienting the  $\beta$ -loops to points we only quotient the disk with basepoint in the branch direction of each of the  $\beta$ -loops. Since the basepoint is collapsed from a circle, the collapsed regions are all bounded by the circle. However, back on the branched surface the circle is either a boundary circle, or  $\delta_{cusp}$  bounding the collapsed regions opposite its branch direction. Hence by collapsing loops we are not collapsing any sink disk. On the other hand, the  $\alpha$ -bigon we collapsed is bounded by  $\alpha$  opposite its branch direction, so we didn't collapse any sink corner. Hence no sink disk is collapsed by our operations. However, we did collapse the double points in pairs (that are originally connected by  $\beta$ -arcs in the  $(\alpha, \delta)$ -source bigon, see  $Q, R$  in Figure 22 for an example), so in the 4-pointed sphere after collapsings each intersection of  $(\alpha, \beta)$  correspond to two sink corners, see the fifth picture of Figure 24.

### Step 3: Set up “sink tube push” for the rational tangle

We now spot possible sink disks on  $(S, a, b, c, d)$  after collapsings. Notice that now for any sector on  $S$  with a boundary  $\alpha$ -arc, its boundary  $\alpha$ -arc would have branch direction pointing inwards (we've collapsed the other side of  $\alpha$ ). So to check if a sector on  $S$  is a sink disk, we only need to check the branch direction of its boundary  $\beta$ -arcs. See the shaded region in Figure 25.(a) for an example of sink disks here. We still need to push  $\beta$ -arcs on  $S$  to eliminate such sink disks. Now that  $S$  is obtained by cutting  $\Sigma^+$  along  $\delta$  and collapsing, when pushing  $\beta$ -arcs on  $S$  we automatically won't push across  $\delta$ . Hence we only need to guarantee that we do not move the  $\beta$ -boundary arc of the  $(\alpha, \beta)$ -source bigon. This arc, after the collapsings, is now the point  $e$  as shown in Figure 24 and Figure 25.(a). It is the  $(\alpha, \beta)$ -intersection that is closest to  $a$ . In our following pushings, we'll treat it as an anchor for  $\beta_c$ , since it can never be moved.

Since the  $\alpha$ -arc does intersect  $\beta_c$  at  $e$ , which is not a basepoint, we know  $q \geq 2$ , and thus  $p \geq 1$ . **We claim that if  $p = 1$ , then there's already no sink disk.** In fact, suppose we start tracing the  $\beta_c$ -arc from  $d$ ; then since it will not intersect horizontal frames  $ad$  and  $bc$  again before getting to the endpoint, it will necessarily wind from  $d$  all the way down to the bottom, see Figure 24 bottom-right. Hence  $\beta_c$  always intersects  $\alpha$  in the same direction. Now consider the segments of the  $\alpha$ -arc cut out by  $\beta$ . We claim that none of them is the boundary arc of a sink disk. In fact, except the segments with an endpoint  $a$  or  $b$ , all other segments are “ $\beta$ -parallel” in a similar sense as Definition 2.1, thus cannot appear on the boundary of a sink disk. For the segment with an endpoint  $b$ , we notice that back on  $\Sigma^+$  it is attached to a circle at  $b$ . According to our construction, this circle is either the boundary circle  $\delta_{\partial_h}$ , or a branch locus circle, whose branch direction points to the other side (i.e. not the side our  $\alpha$ -segment is attached to). Either way our  $\alpha$ -segment cannot be a boundary arc of a sink disk. The segment with endpoint  $a$  is  $ae$  coming from the removed source bigon, so actually is not part of the branch locus. It follows that no sink corners at the  $(\alpha, \beta)$ -intersections are actually sink disks, and hence

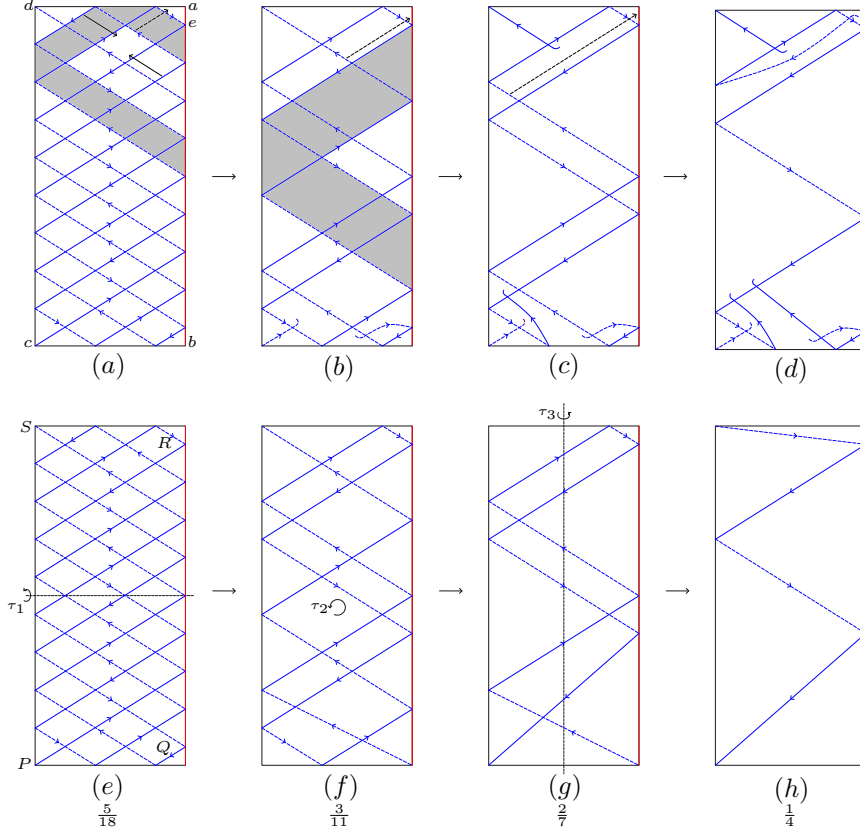


FIGURE 25. Reducing rational tangles

our branched surface (obtained by doing sink tube push to  $\mathcal{A}''$ ) is already sink disk free. **From now on we suppose  $p \geq 2$ .**

We show that, for  $\beta_c$  in standard position on  $(S, a, b, c, d)$  we can again define a “sink tube” to push. We can regard the boundary of the rectangle  $abcd$  as a simple closed curve on  $S$ . We call this curve  $(a - b - c - d - a)$  the (smoothed) **frame circle** and denote it as  $\epsilon$ . Now  $\beta_c$  and  $\epsilon$  together cut  $S$  into pieces (we remark that vertices of these pieces are the intersection points of  $\beta_c$  and  $\epsilon$ , so basepoints are not necessarily vertices). Since the  $\beta$ -arc is oriented, we can define  $\beta$ -sink, source, and parallel arcs similarly as in Definition 2.1 for the  $\epsilon$ -arcs cut out by  $\beta$ . And then we can define  $\beta$ -sink, source, and parallel sectors for the quadrilateral pieces of  $S$  cut out by  $\beta_c$  and  $\epsilon$ . In fact, if we first cut along  $\epsilon$  and then along  $\beta_c$ , we can see that we first cut  $S$  into two disks, and then cut the disks with parallel  $\beta$ -arcs; hence we’re getting mostly quadrilateral pieces, except for certain “bigons” near the basepoints, see Figure 25.(a). (More precisely, for each of the bigons obtained by cutting disks with parallel  $\beta$ -arcs, we see a basepoint in the interior of its  $\epsilon$ -boundary; we say this bigon is **near** the basepoint.)

There are two basepoints that are endpoints of  $\beta$  and two basepoints that are not. For each of the two non-endpoints, we notice that the  $\epsilon$ -arc containing them do not contain an entire edge of the rectangle (if it does, then  $\beta_c$  would intersect that edge only once at the basepoint, contradicting the fact that  $p, q \geq 2$ ). It

follows that the  $\epsilon$ -arc appears on the boundary of a bigon on one side and a  $\beta$ -sink or source sector on the other, see Figure 26.(a), where we flattened the bubbled rectangle near the basepoints. Still, we call the bigon a sink (resp. source) bigon if the boundary  $\epsilon$ -arc is  $\beta$ -sink (resp. source).

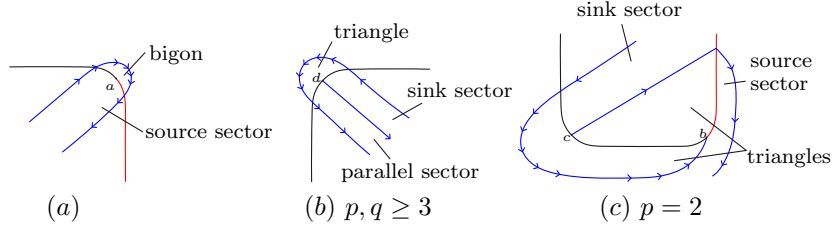


FIGURE 26. Bigons and Triangles at the basepoints

On the other hand, for each of the two endpoints, the “bigon” near it is actually a triangle since the endpoint itself is also a vertex, see Figure 26.(b)(c). When both  $p, q \geq 3$ , neither of the two  $\epsilon$ -edges of the triangle is a whole edge of the rectangle  $abcd$ , so they each bound a quadrilateral on the other side. Moreover, as shown in Figure 26.(b), one of them is a parallel sector and the other is a sink or source sector. When  $p = 2$  or  $q = 2$  (notice it can't be both since  $(p, q) = 1$ ), the two triangles corresponding to endpoints share an  $\epsilon$ -edge, which is actually an entire edge of the rectangle  $abcd$ . Moreover, since that  $\beta_c$  has  $(p + q - 2)$  intersections with  $\epsilon$  other than the endpoints, and that exactly one of  $p, q$  is even (they are coprime and one equals 2 by our case supposition), away from endpoints  $\beta_c$  intersects  $\epsilon$  in an odd number of times. Hence near the endpoints the  $\beta_c$ -threads are on different sides of  $\epsilon$ , see Figure 26.(c). Now by our definition the shared  $\epsilon$ -edge of the two triangles is  $\beta$ -parallel, and the two quadrilaterals bounded by the not-shared  $\epsilon$ -edges of the two triangles are exactly one sink sector and one source sector, as in Figure 26.(c).

Recall that in the (1,1)-diagram case, we're able to define the sink tube since there're only two  $\beta$ -sink arcs among the boundary  $\alpha$ -arcs of non-quadrilateral pieces (so that one is eventually connected to the other by pasting  $\beta$ -sink sectors). To establish a similar theory for  $(S, \beta_c, \epsilon)$ , we need to verify the same thing, i.e. there're only two  $\beta$ -sink arcs among the boundary  $\epsilon$ -arcs of the bigons and triangles. We achieve this by introducing symmetries of  $\beta_c$  on  $(S, a, b, c, d)$ . One should think of this as an analogue to the hyperelliptic involution in the (1,1)-diagram case.

There are  $\pi$ -rotations of  $S$  that keeps  $\epsilon$  invariant, while interchanging the basepoints in pairs. We regard  $(S, a, b, c, d)$  as the bubbled rectangle, and define  $\tau_1 \sim \tau_3$  as in Figure 25.(e)  $\sim$  (g). More precisely,  $\tau_1, \tau_3$  interchanges the front rectangle and the back rectangle, and then on each rectangle acts as a reflection along the axis;  $\tau_2$  keeps the front and back rectangles invariant, while acts as a  $\pi$ -rotation or central reflection on each rectangle. We see that  $\tau_1$  interchanges the basepoints  $a, b$  and  $c, d$ ,  $\tau_2$  interchanges  $a, c$  and  $b, d$ , and  $\tau_3$  interchanges  $a, d$  and  $b, c$ .

**Claim.** If the endpoints of  $\beta_c$  are interchanged by  $\tau_{i_0}$ , then  $\tau_{i_0}(\beta_c)$  is isotopic to  $\beta_c$  on  $(S, a, b, c, d)$ , but has its orientation reversed.

*Proof of the claim.* Since  $\beta_c$  and  $\epsilon$  are in tight position on  $(S, a, b, c, d)$ , we know  $\tau_{i_0}(\beta_c)$  and  $\tau_{i_0}(\epsilon) = \epsilon$  are also in tight position. Hence  $\tau_{i_0}(\beta_c)$  is also characterized by a rational number  $\frac{p'}{q'}$ ,  $p', q' \geq 0$  and  $(p', q') = 1$ . Now since  $\tau_{i_0}$  interchanges the basepoints, it sends the rectangle edge  $ab$  to either itself or  $cd$ . Let  $\text{IC}(\beta_c, ab)$  be the intersection count of  $\beta_c$  and  $ab$ , where we recall we count 1 for each basepoint intersection and 2 for each non-basepoint intersection. Noticing that  $\text{IC}(\tau_{i_0}(\beta_c), ab) = \text{IC}(\tau_{i_0}(\beta_c), cd) = q'$ , we have

$$q = \text{IC}(\beta_c, ab) = \text{IC}(\tau_{i_0}(\beta_c), \tau_{i_0}(ab)) = \text{IC}(\tau_{i_0}(\beta_c), ab) = q'.$$

Similarly we can show  $p = p'$ . Hence  $\tau_{i_0}(\beta_c)$  is actually isotopic to  $\beta_c$  on  $(S, a, b, c, d)$ . Moreover, since  $\tau_{i_0}$  interchanged the endpoints of  $\beta_c$ , the starting point of our oriented  $\tau_{i_0}(\beta_c)$  is actually the ending point of  $\beta_c$ , and hence the orientation is reversed.  $\square$

The claim gives us the symmetry of  $\beta_c$  we need. According to the endpoints of our  $\beta_c$ , we can pick a suitable  $\tau_{i_0}$  interchanging its endpoints. Now since our  $\tau_{i_0}$  reverses the orientation of  $\beta_c$ , a  $\beta$ -sink arc is mapped to a  $\beta$ -source one, so the  $\tau_{i_0}$  image of a sink bigon is a source bigon and vice versa. Since there are exactly 2 bigons, there are exactly one sink bigon and one source bigon. Similarly, there are exactly one triangle with a  $\beta$ -sink  $\epsilon$ -edge and one triangle with a  $\beta$ -source  $\epsilon$ -edge (recall a triangle always contains a  $\beta$ -parallel  $\epsilon$ -edge). Hence for all the non-quadrilateral regions, there are only two boundary  $\epsilon$ -arcs that are  $\beta$ -sink (resp. source). It then follows that the two arcs must be connected by pasting  $\beta$ -sink (resp. source) sectors along the boundary  $\epsilon$ -arcs. Thus we can still define the **sink (resp. source) tube** here, and a statement parallel to Proposition 2.5 still holds.

We now introduce the “sink tube push” in this case. Recall that since we’ve already cut along  $\delta$ , when pushing the arcs we only need to make sure that we do not move the boundary  $\beta$ -arc of the source bigon, or the point  $e$  after collapsings as in Figure 25.(a). We used to guarantee this by manually spot the source bigon at one of the long  $\beta$ -arcs of the sink tube, but for our rational tangles there is a more natural way. One can define each  $\beta$ -segment cut out by  $\epsilon$  to be of length 1. By the previously discussed symmetry of  $\beta_c$  we can describe it as Figure 27.(a) upper-left, where  $P, S$  are endpoints of  $\beta_c$ ,  $Q$  is the midpoint of the boundary  $\beta$ -arc of the sink bigon, and  $R$  the midpoint of the boundary  $\beta$ -arc of the source bigon, s.t.  $P, Q, R, S$  appear in order and  $d(P, Q) = d(R, S)$ . We then define our “sink tube push” to push the long  $\beta$ -arc of the sink tube in  $PQ$  onto the other long  $\beta$ -arc in  $QS$ . Moreover, we modify our operation at the ends of the tube, so that near the  $\beta$ -sink bigon we obtain a  $\beta$ -loop bounding a basepoint (see bottom-right corner of Figure 25.(a)(b), or Figure 27.(b)), and near the triangle with  $\beta$ -sink edge containing  $P$  we push the  $\beta$ -arc connected to  $P$  onto the  $\beta$ -edge of the triangle (see the bottom-left corner of Figure 25.(a)(b), or the first arrow in Figure 27.(c)). Since  $e$  is a vertex of the source bigon,  $d(e, R) = 1/2$ . Since  $R$  is not on  $PQ$ ,  $e$  is also not on  $PQ$ . Thus our operation does not move  $e$  and is hence a legal push.

We now show that the new double points created by our sink tube push for  $\beta_c$  are all safe. There are two new double points:  $X_q$  on the new  $\beta$ -loop  $\beta_q$  near  $Q$ , and  $X_p$  on the  $\beta$ -edge of the triangle near  $P$ , which is connected to  $P$  by a short arc in the triangle, see Figure 27.(b)(c). Every sink corner of possible double points on  $\beta_q$  has the basepoint inside on its boundary (there might be double points other than  $X_q$  if the basepoint is  $b$ , where  $\alpha$  intersects  $\beta_q$ ). Since  $a$  is on the boundary

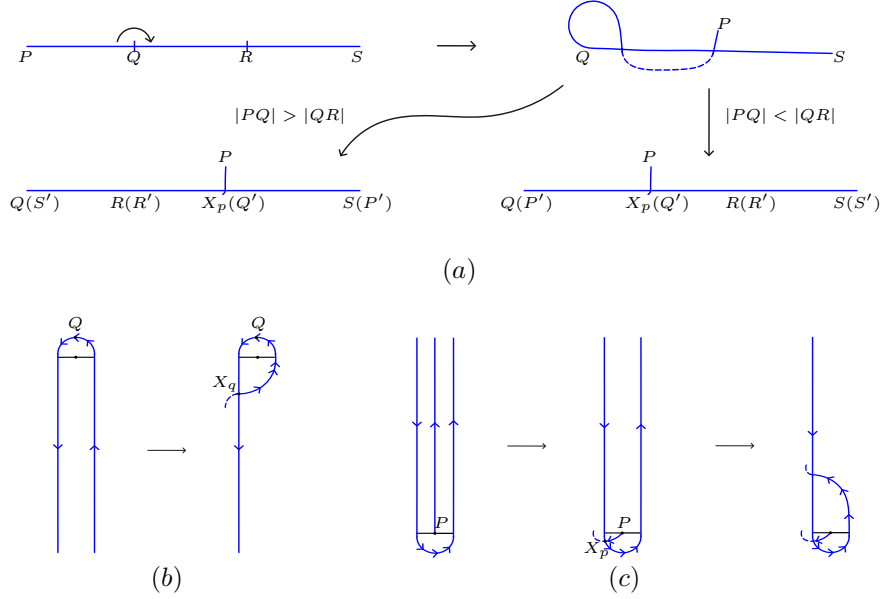


FIGURE 27. Sink tube push for rational tangles

of the source bigon (of  $(S, \beta_c, \epsilon)$ ), the basepoint inside  $\beta_q$  cannot be  $a$ . Hence it is obtained by collapsing a circle. Again, back on  $\Sigma^+$  the circle before collapsing is either a boundary circle of the branched surface or a branch locus circle whose branch direction points to the other side. Sink corners of double points on  $\beta_q$  all have part of this circle on boundary, thus cannot be sink disks. The sink corner of  $X_p$  has a boundary arc  $PX_p$ , and thus has the basepoint  $P$  on its boundary. Now since  $P$  is an endpoint of  $\beta_c$ , it is not  $a$ , and is hence obtained by collapsing a  $\beta$ -loop. Yet again, back on  $\Sigma^+$  the sink corner of  $X_p$  has a boundary arc belonging to this collapsed loop, where the branch direction points to the other side. It follows that  $X_p$  is also safe.

We do a further collapsing to prepare for the next step. Since double points on  $\beta_q$  are all safe, we can further collapse (or quotient)  $\beta_q$  and the disk it bounds in its branch direction on  $S$  to the basepoint inside, without destroying possible sink disks. See Figure 27.(a). For the purpose of the next step, we describe a **complete** “sink tube push” procedure for a rational tangle to include both the arc-pushing and the collapsing of the loop afterwards.

**Step 4: Perform sink tube push repeatedly to eliminate sink disks**

Unfortunately, only one sink tube push for  $\beta_c$  is unlikely to eliminate all sink disks, see the shaded region of Figure 25.(b) for a sink disk that remains after the sink tube push. Our strategy is to perform sink tube pushes repeatedly until when we can guarantee that there is no sink disks left. To do this we need to obtain a new  $\beta$ -arc connecting basepoints.

Now if we temporarily ignore the short  $\beta$ -segment  $PX_p$  (we call it a **tail**), we get a new  $\beta$ -arc  $\beta'_c$  connecting  $Q$  and  $S$  (see Figure 27.(a) upper-right, notice the loop at  $Q$  is collapsed). This  $\beta'_c$  is represented by some rational number  $\frac{s}{t}$ , where

$s, t \geq 0$ ,  $(s, t) = 1$  and  $s + t < p + q$  (the number of intersections is decreasing at least by 1 by collapsing the  $\beta$ -loop at  $Q$  to the basepoint). Moreover, if  $s, t \geq 2$ , we still can define the sink tube for  $(S, \beta'_c, \epsilon)$ . Since we ignore the tail  $PX_p$ ,  $P$  is no longer a vertex, and thus the triangle of  $(S, \beta_c, \epsilon)$  at  $P$  turns to a bigon of  $(S, \beta'_c, \epsilon)$ ; in fact, the triangle with a **sink**  $\epsilon$ -edge becomes the **sink** bigon of  $(S, \beta'_c, \epsilon)$ , as shown in the middle picture of Figure 27.(c). On the other hand, the source bigon of  $(S, \beta'_c, \epsilon)$  is the same as the source bigon of  $(S, \beta_c, \epsilon)$  at  $R$ . Depending on whether  $d(P, Q) > d(Q, R)$  or  $d(P, Q) < d(Q, R)$  (they cannot be equal since  $d(P, Q)$  contains a half length at  $Q$  while  $d(Q, R)$  contains two halves at both ends and is thus an integer), we can set new  $P', Q', R', S'$  as in the bottom two pictures of Figure 27.(a) (we remark that one can identify  $Q'$  the midpoint of the boundary  $\beta$ -arc of the new sink bigon with  $X_p$ ). We can then do a “sink tube push” for  $\beta'_c$ , pushing our new  $P'Q'$  onto  $Q'S'$ , in the same sense as before. Notice that since the tail  $PX_p$  is inside the new sink bigon, it is not moved or moved over by our new push, see the third picture of Figure 27.(c) (hence we’re good to first ignore the tail and define sink tube push with  $\beta'_c$ ).

It is still true that the new double points created by pushing  $\beta'_c$  are safe. We still get two new double points:  $X'_q$  on the new loop  $\beta'_q$  near  $Q'$ , and  $X'_p$  connected to  $P'$  by another short arc. In fact, the only difference from the  $\beta_c$  case is the tail inside  $\beta'_q$ . However, with or without the tail, all sectors inside the small disk bounded by  $\beta'_q$  in its branch direction have the basepoint  $P$  on their boundaries. Again and again, back on  $\Sigma^+$  these sectors have boundary arcs on a branch locus circle collapsed to  $P$ , whose branch direction points outwards to the other side, see Figure 28. It follows that the sink corners of possible double points on  $\beta'_q$  cannot be sink disks; in particular  $X'_q$  is safe. By essentially the same argument as the  $\beta_c$  case we can show that  $X'_p$  is also safe.

Since in fact all double points on  $\beta'_q$  are safe, we can still collapse this loop and the small disk it bounds to the basepoint  $P$  inside, without collapsing sink disks. This way we successfully defined another *complete* sink tube push procedure.

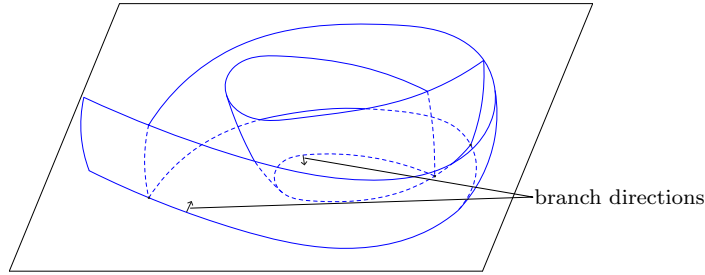


FIGURE 28. Nested  $\beta$ -circles to be collapsed

If we ignore the tail from the new  $\beta'_c$ -sink tube push, we get yet another  $\beta$ -arc connecting basepoints. It follows that we can *repeatedly* perform *complete* “sink tube push” procedures for rational tangles, without getting new double points that’re not safe or collapsing existing unsafe double points, whenever the rational tangle  $\frac{p}{q}$  with  $(p, q) = 1$  representing the  $\beta$ -arc has  $p, q \geq 2$ . Each sink tube push creates a new tail. However, the tail is in the sink bigon of the next sink tube

push (if there is a next one), and will be enclosed in loop and collapsed by the next (complete) sink tube push. See Figure 25 for an example.

We remark that the endpoints of  $\beta$ -arc changes as the rational tangle changes. In fact, the endpoints of  $\beta$  is determined by the parity types of the rational number: if the rational number is odd/even, then the endpoints of  $\beta$ -arc are  $c, d$ , if odd/odd, then the endpoints are  $b, d$ , and if even/odd endpoints are  $b, c$ . We also remark that our sink tube push can be performed regardless of the location of the endpoints, as long as the source bigon is at  $a$ .

Since  $p+q$  is decreasing, this process of repeated complete sink tube pushes will terminate. It terminates when either  $p = 1$  or  $q = 1$ . We show that now every double point on  $S$  is safe. The remaining  $\beta$ -arcs on  $S$  contains a rational tangle connecting two basepoints of the three  $\{b, c, d\}$ , and a tail from the last sink tube push (notice we're not able to further enclose this in a loop and collapse). However, the double point on this tail is safe (connected to a basepoint), so we still only need to pay attention to the double points from the intersection of  $\alpha$  and the  $\beta$ -rational tangle arc. If  $q = 1$ , then  $\alpha$  and  $\beta$  only intersects at  $b$ ; but this is impossible, since our anchor  $e$  is not moved and serves as another intersection. Hence  $p = 1$ . Now similarly as our argument before (at the beginning of Step 3), the  $\beta$ -rational tangle arc intersects  $\alpha$  always in the same direction, and all double points are safe. It then follows that after our repeated operations we get a branched surface  $\mathcal{A}'''$  that has no sink disk.

We are now in position to apply Lemma 2.9. We claim that no horizontal boundary component of  $\mathcal{A}'''$  is a disk. Since our splittings are always along disks and modelled on Figure 17 middle, they do not change the topology of the horizontal boundary, hence we only need to check for  $\mathcal{A}''$ . Now consider horizontal boundary components of  $\mathcal{A}''$  (with boundary). The boundary of these horizontal boundary components must correspond to the boundary or branch locus of  $\mathcal{A}''$ . For the boundary circle of  $\mathcal{A}''$  corresponding to the  $\mathcal{C}'$ -cusp, there are two components of horizontal boundary bounded by it, each homeomorphic to  $\partial_h^\pm$  (they're the sides of  $\partial_h^\pm$  that  $\mathcal{A}$  is not attached to), thus not being a disk. Other possible boundary circles are  $\delta$ , the  $(\alpha, \beta)$ -cusp, and the boundary circle in the sink bigon - exactly the cusps and boundary circles that remain in  $\mathcal{B}'$ . Hence for a disk horizontal boundary component in  $\mathcal{A}''$ , we can find a corresponding disk of contact in the regular neighborhood of  $\mathcal{B}'$ . However,  $N(\mathcal{B}')$  is homeomorphic to the (1,1)-knot complement, and we recall from proof of Lemma 3.11 that all the boundary circles and cusps of  $\mathcal{B}'$  correspond to the meridian of the knot. Our claim then follows from the fact that there's no disk bounded by meridian in the nontrivial knot complement.

Also since  $\mathcal{B}'$  is co-oriented, it cannot carry a sphere or a torus, for they will then be non-separating in the total lens space. Hence  $\mathcal{A}'''$  also cannot carry any sphere or torus. Now we can use Lemma 2.9 and conclude that  $\mathcal{A}'''$  fully carries a lamination. Hence  $\mathcal{A}''$  also fully carries a lamination.  $\square$

**3.5. Finishing the proof.** We finish this section by proving Proposition 3.10 and Proposition 3.1.

*Proof of Proposition 3.10.* By Lemma 3.14 and Lemma 3.13 we know  $\mathcal{A}'$  fully carries a lamination. Since  $\mathcal{C}$  fully carries a lamination by our hypothesis,  $\mathcal{C}'$ , obtained

by removing a disk in the interior of a sector of  $\mathcal{C}$ , also fully carries a lamination. Now by Lemma 3.12 and Lemma 3.11  $\mathcal{B}$  fully carries a lamination, as required.  $\square$

*Proof of Proposition 3.1.* Let  $(\Sigma, \alpha, \beta, z, w)$  be a nontrivial reduced (1,1)-diagram. If it's primitive, then by Proposition 3.4 the associated branched surface fully carries a lamination. If it is not, then by Proposition 3.9 one can replace one of the curves by the curve carrying it, to get another nontrivial reduced (1,1)-diagram. Let's say we replace  $\alpha$  by  $\gamma$ , and place  $\alpha$  in standard position. Since the original reduced (1,1)-diagram is nontrivial, there are rainbow  $\beta$ -arcs. It follows that the number of intersection points of  $\gamma$  and  $\beta$  is strictly less than that of  $\alpha$  and  $\beta$ , since  $\gamma$  only intersects the vertical  $\beta$ -arcs (see Figure 10). One can always do such replacement when the diagram is not primitive, but can only do it for finite times according to the observation above. Eventually we get a finite sequence of reduced (1,1)-diagrams with the terminal one primitive. Now by Proposition 3.10 and induction every reduced (1,1)-diagram in this sequence has its associated branched surface fully carrying laminations.  $\square$

#### 4. CO-ORIENTED TAUT FOLIATIONS FROM LAMINATIONS

In this section we construct co-oriented taut foliations in (1,1)-knots complements.

*Proof of Theorem 1.3.* Let  $(\Sigma, \alpha, \beta, z, w)$  be some nontrivial reduced (1,1)-diagram representing the nontrivial (1,1)-knot, and  $\mathcal{B}$  be the associated branched surface. Notice that we actually have  $N(\mathcal{B})$  homeomorphic to the knot complement  $M$  by Lemma 2.13. Now by Proposition 3.1,  $\mathcal{B}$  fully carries some lamination  $\mathcal{L} \subset N(\mathcal{B})$ , and by blowing up leaves we can further assume  $\partial_h N(\mathcal{B}) \subset \mathcal{L}$ . Since our  $\mathcal{B}$  is co-oriented by definition, components of  $N(\mathcal{B}) - \mathcal{L}$  are trivial  $I$ -bundles over oriented surfaces, and  $\mathcal{L}$  extends to a co-oriented foliation  $\mathcal{F}$  of  $N(\mathcal{B})$ .

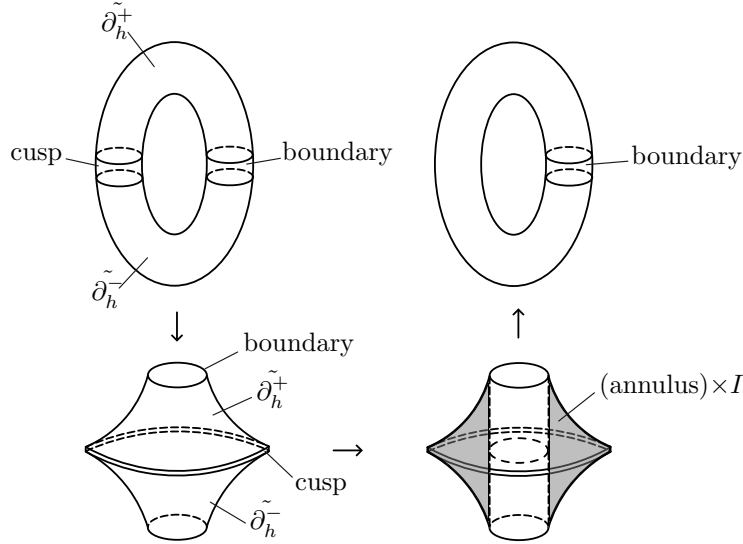


FIGURE 29. Attaching thickened annulus

Foliation  $\mathcal{F}$  is tangent to the boundary torus of  $N(\mathcal{B})$  at the two annuli horizontal boundary components  $\tilde{\partial}_h^+, \tilde{\partial}_h^-$ , and transverse to the cusp and boundary of  $\mathcal{B}$ , or the vertical boundary of  $N(\mathcal{B})$ . Moreover, the annulus coming from the cusp is foliated by product. We can thus extend  $\mathcal{F}$  by attaching some  $(\text{annulus} \times I)$  (foliated trivially by the annuli) to the cusp, connecting the two annuli horizontal boundary components. (See shaded part of Figure 29.) The new foliation  $\mathcal{F}'$  still foliates a 3-manifold homeomorphic to  $M$ , and intersects the boundary torus transversely in a suspension foliation of the meridional slope, with possible nontrivial holonomy at the annulus coming from the circle boundary of  $\mathcal{B}$ , and product foliation elsewhere.

It remains to show that  $\mathcal{F}'$  is taut (it is co-oriented since  $\mathcal{F}$  is). In fact, to each  $I$ -fiber of  $N(\mathcal{B})$  we can take a transverse arc connecting its endpoints in the  $(\text{annulus} \times I)$  attached; thus by joining the  $I$ -fiber with this arc we get a closed transverse circle. Since each leaf of  $\mathcal{F}'$  must pass through some  $I$ -fiber of  $N(\mathcal{B})$ , to each leaf there is a transverse circle passing through it, and  $\mathcal{F}'$  is hence taut.  $\square$

## REFERENCES

- [BGH21] Steven Boyer, Cameron McA Gordon, and Ying Hu. Slope detection and toroidal 3-manifolds. *arXiv preprint arXiv:2106.14378*, 2021.
- [Eft18] Eaman Eftekhary. Bordered floer homology and existence of incompressible tori in homology spheres. *Compositio Mathematica*, 154(6):1222–1268, 2018.
- [Gab92] David Gabai. Taut foliations of 3-manifolds and suspensions of  $S^1$ . *Annales de l'Institut Fourier*, 42(1-2):193–208, 1992.
- [GO89] David Gabai and Ulrich Oertel. Essential laminations in 3-manifolds. *Annals of Mathematics*, 130(1):41–73, 1989.
- [HRW23] Jonathan Hanselman, Jacob Rasmussen, and Liam Watson. Bordered floer homology for manifolds with torus boundary via immersed curves. *Journal of the American Mathematical Society*, 2023.
- [HS89] Andrew Haas and Perry Susskind. The geometry of the hyperelliptic involution in genus two. *Proceedings of the American Mathematical Society*, 105(1):159–165, 1989.
- [Li02] Tao Li. Laminar branched surfaces in 3-manifolds. *Geometry & Topology*, 6(1):153–194, 2002.
- [Li24] Tao Li. Taut foliations of 3-manifolds with heegaard genus 2. *Duke Mathematical Journal*, 173(8):1427–1475, 2024.
- [OS10] Peter S Ozsváth and Zoltán Szabó. Knot floer homology and rational surgeries. *Algebraic & Geometric Topology*, 11(1):1–68, 2010.
- [Ras05] Jacob Rasmussen. Knot polynomials and knot homologies. *Geometry and Topology of Manifolds*, pages 261–280, 2005.